

# CHALMERS



*Modeling and Measurements of Transformer Behavior at Different Voltages and Frequencies*

*Master of Science Thesis in the Master Degree Program, Electric Power Engineering*

MATTIAS PERSSON

WAQAS BAIG

Department of Energy and Environment  
*Division of Electric Power Engineering*  
CHALMERS UNIVERSITY OF TECHNOLOGY  
Göteborg, Sweden, 2011

# Modeling and Measurements of Transformer Behavior at Different Voltages and Frequencies

MATTIAS PERSSON

WAQAS BAIG

Department of Energy and Environment  
CHALMERS UNIVERSITY OF TECHNOLOGY  
Göteborg, Sweden, 2011

## Abstract

This master thesis deals with the modeling and measurements of transformer behavior when it is subjected to abnormal supply voltages and frequencies. The analysis has been performed on a three and a five limb transformer rated at 4 kVA each. The transformer model was implemented in MATLAB<sup>®</sup> with a two-axis model (Park model) taking saturation into account. Experimental tests were performed in a laboratory setup to validate the model. The transformers and the model were subjected to different swells and dips while supplying both inductive and resistive loads.

The proposed model produces results that are consistent with the experimental ones with an average error of 2%. The experimental result from a voltage dip of 100 ms indicates that the inrush current drawn by the two transformers differ and it depends strongly on the type of loading and the type of transformer. Thus, for a pure inductive load, the transformer draws 7 pu as compared to 5.3 pu for three and five limb transformer respectively. For 50% resistive loading, the value of inrush current is reduced to 2.6 pu and 1.5 pu respectively.

The results from four selected voltage profiles are presented and evaluated. Besides this, the final model along with the methods to extract parameters including  $L_m$  is presented in the report. It is concluded that five limb transformer are less affected by voltage dips and swells as compared to three limb transformer. The authors have also suggested improvements to the current model and future work.

## Acknowledgements

The authors would like to express their deepest gratitude to Professor Torbjörn Thiringer, our thesis supervisor for invaluable advice and excellent supervision.

We would also like to gratefully acknowledge guidance and consultation offered by Daniel Karlsson and Bertil Svensson from Gothia Power AB. A bundle of appreciation also goes to Per Norberg from Chalmers University of Technology and Fredrik Heyman from OKG AB for providing the opportunity and the funding to undertake this Master thesis.

Many thanks go to Aleksander Bartnicki from Chalmers University of Technology for his splendid support during laboratory tests. His practical advice and laboratory safety instructions truly refined our skills.

High appreciation is offered to Dr. Massimo Bongiorno from Chalmers University of Technology for his utmost support for setting up the laboratory and valuable technical advice.

Many useful discussions with the staff members and colleagues at Chalmers University of Technology proved to be extremely helpful to nurture new ideas, which include Mebtu Beza, Tarik Abdulahovic and Eva Palmberg in particular.

Last but not the least; we would like to thank our friends and families for their motivation and support.

Waqas Baig

Mattias Persson

Göteborg, Sweden, December 2011.

## List of Symbols

Symbol	Parameter	Unit
$R_p$	resistance of primary winding	$\Omega$
$R_s$	resistance of secondary winding	$\Omega$
$L_{p\lambda}$	leakage inductance of primary winding	H
$L_{s\lambda}$	leakage inductance of secondary winding	H
$L_m$	magnetizing inductance	H
$V_{L-L,RMS}$	line-line RMS voltage	V
$u_p$	primary voltage	V
$i_p$	primary current	A
$R_p$	resistance of primary series branch	$\Omega$
$\omega_k$	angular speed of coordinate system	rad/s
$\psi_p$	primary flux linkage	Wb
$u_s$	secondary voltage	V
$i_s$	secondary current	A
$R_s$	resistance of secondary series branch	$\Omega$
$\psi_s$	secondary flux linkage	Wb
$L_p$	primary inductance of series branch	H
$L_s$	secondary inductance of series branch	H
$L_m$	magnetizing inductance of parallel branch	H
$L_{p\lambda}$	primary leakage inductance	H
$L_{s\lambda}$	secondary leakage inductance	H
<b>A</b>	system matrix	
<b>B</b>	input matrix	

<b>y</b>	output matrix	
<b>I</b>	current column matrix	A
<b>L</b>	inductance matrix	H
<b>R</b>	resistance matrix	$\Omega$
<b>U</b>	voltage column matrix	V
$X_m$	magnetizing reactance of parallel branch	H
$i_m$	magnetizing current of parallel branch	A
$U_{dc}$	dc voltage signal	-
$V_{dc}$	dc voltage	V
$V_{ac}$	ac voltage	V
$I_{dc}$	dc current	A
$V_{oc}$	open circuit voltage	V
$V_{sc}$	short circuit voltage	V
$I_{oc}$	open circuit current	A
$I_{sc}$	short circuit current	A
$P_{oc}$	open circuit power	W
$P_{sc}$	short circuit power	W

## Abbreviation

## Meaning

RMS	root mean squared
$j$	imaginary number
V-I curve	voltage current curve
kVA	kilo volt ampere
RTI	real time interface
OSRCC	opto sending and receiving conversion card
CT	current transformer
pu	per-unit
dq	direct-quadrature coordinate system
abc	three phase system
L-L	line-Line
L-N	line-neutral
$V_{ref}$	reference voltage

## Table of Contents

1. Introduction.....	1
1.1. Background .....	1
1.2. Previous Work.....	1
1.3. Purpose .....	2
2. Theory.....	3
2.1. Three Phase Three Limb Transformer .....	3
2.2. Three Phase Five Limb Transformer .....	3
2.3. Open Circuit Zero Sequence Impedance .....	4
2.3.1. Three Phase Three Limb Transformer .....	4
2.3.2. Three Phase Five Limb Transformer .....	5
2.4. Transformer Losses.....	5
2.4.1. Eddy Currents Loss.....	5
2.4.2. Hysteresis Loss .....	5
2.4.3. Winding Loss .....	6
3. Case Set-Up .....	7
3.1. Voltage Profiles .....	7
3.2. Description of Transformers .....	9
3.3. Determination of Transformer Parameters.....	10
3.3.1. Open Circuit and Short Circuit Test.....	10
3.3.2. Magnetizing Inductance Test.....	11
3.4. Determination of Loads .....	12
3.4.1. Calculation for Loads.....	12
3.5. Model .....	14
3.5.1. Park Model Transformer Model .....	14

3.5.2. Three Phase Transformer Model .....	15
3.5.3. Implementation in MATLAB.....	16
3.5.4. Saturation Modeling .....	16
3.6. Laboratory Set Up .....	18
3.6.1. Real-Time Interface: d-SPACE .....	19
3.6.1.1. d-SPACE Interface box .....	20
3.6.1.2. Measurement card and OSRCC .....	21
3.6.1.3. Measurement Box .....	23
3.6.1.4. Inverter .....	23
3.7. Measurement Accuracy / Errors .....	26
4. Analysis.....	27
4.1. Base Case: Three Phase 3 Limb Transformer.....	28
4.1.1. Effect of Variation of Load for 3 Limb Transformer.....	29
4.1.1.1. Voltage Profile 2 .....	29
4.1.1.2. Voltage Profile 3 .....	31
4.2. Comparison between Simulation and Experimentation for 3 Limb Transformer .....	32
4.3. Comparison between 3 and 5 Limb Experimental results.....	33
4.3.1. Voltage Profile 2 – Secondary Voltages .....	33
4.3.2. Voltage Profile 3 – Secondary Voltages .....	34
4.3.3. Voltage Profile 2 – Primary Voltages and Currents .....	34
4.4. Inrush Current Comparison Between 3 and 5 Limb.....	36
4.5. Window Test .....	38
4.5.1. Comparison of Window Test for 3 Vs 5 Limb.....	39
5. Conclusion .....	41
6. Future Work .....	42

References..... 43

Appendix A. Parameter Extraction ..... 45

    Rating plate ..... 45

    67128 – 5 limb transformer ..... 45

    67129 – 3 limb transformer ..... 45

    Open circuit test ..... 45

    Short circuit test ..... 46

    Calculations ..... 46

    Magnetizing inductance test ..... 47

Appendix B. Measurement Devices ..... 50

Appendix C. Additional Results ..... 53

    Voltage profile 1 – Secondary results comparison between three and five limbed transformer. .... 54

    Voltage profile 4 – Secondary results comparison between three and five limbed transformer. .... 55

    Voltage profile 1 – Primary results comparison between three and five limbed transformer..... 56

    Voltage profile 3 – Primary results comparison between three and five limbed transformer..... 57

    Voltage profile 4 – Primary results comparison between three and five limbed transformer..... 58

# 1. Introduction

Transformers are widely used throughout the electric grid and their functionality is primarily to increase or decrease the operational voltage. The behavior of transformers varies with the supplied voltage and frequency. This requires careful understanding of these behaviors so that suitable protection settings are implemented. Thus, any unnecessary tripping of generation or load can be avoided and more stability can be achieved in the overall system.

## 1.1. Background

The dependence on reliable power delivery in the society is increasing. At the same time, disruption of power delivery can result in penalties for the grid owners. At times, this forces the power system to be operating in a more limited operational range. Auxiliary power system is essential for all power plants and safety critical for nuclear power plants. A failure in the auxiliary system can lead to a shutdown of the entire plant. An essential component of this critical system includes the transformers, whose operating features are not well known when subjected to abnormal supply voltages or frequencies. Abnormal supply voltages include voltage dips and voltage swells.

## 1.2. Previous Work

A lot of research has been performed related to the modeling and simulation of transformers. A summary of some of the research papers which are related to the topic are presented.

Some papers build models taking capacitances and core construction differences into account which result in good but complex models ([1], [2], and [3]). Others use validated models built by others but only refer to a specific topology [5].

The behavior of transformers related to their zero sequence impedance for three limb and five limb topology has been studied in [6] and [7].

Different voltage profiles have been investigated by using models in simulation software but there is a lack of comparison to practice in [4].

The need for a simple model along with laboratory tests will provide a good basis for comparison between the two topologies. It will be interesting to make models of the two transformer types and validate them by experimentation.

Research related to dips and loading of transformers and their resulting saturation is discussed in [8].

### **1.3. Purpose**

The purpose of this thesis is to study the response of a transformer when it is subjected to abnormal supply voltages and frequencies. Specifically to be investigated are four voltage profiles which comprise dips and swells of different magnitudes and time duration. These are provided by OKG AB [18]. Moreover, a target is to model the transformer via computer simulations and then simulate different voltage profiles. Furthermore, an aim is to perform the same task practically on a scaled down transformer in a laboratory set-up in which a drive system can be used to vary the supply voltage and frequency to simulate disturbances in the grid. Thus, the above will give an insight into the dynamic and static behavior of a saturated transformer and a comparison between simulation and experiment is to be conducted. For this thesis, the emphasis will be on the analysis of secondary voltages and currents.

## 2. Theory

### 2.1. Three Phase Three Limb Transformer

Three Limb Transformers are commonly used in power and distribution stations for transforming one voltage level to another. A part of the core that is surrounded by windings is called a limb or leg. The remaining part of the core that is not surrounded by windings but is essential for completing the flux path is called the yoke. For each phase, the limbs flux returns through yokes and the two other limbs. The limbs and yokes usually have the same cross-sectional area which implies that the same peak flux flows through the limbs and yokes [9] (Figure 1).

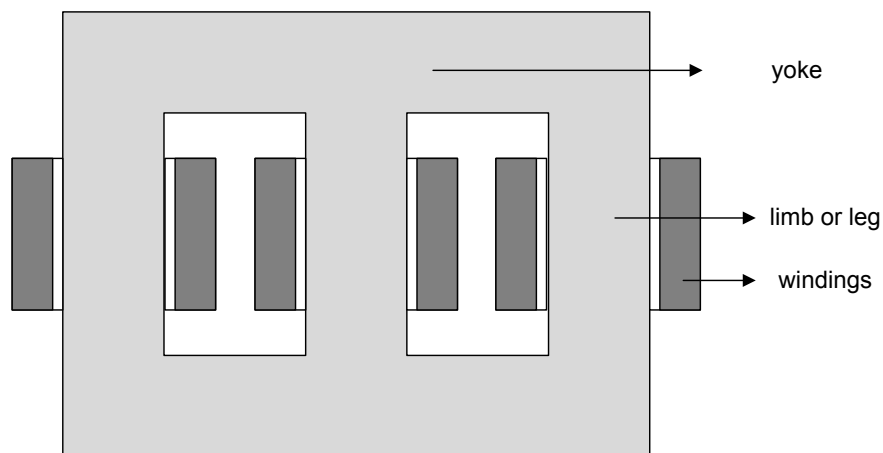
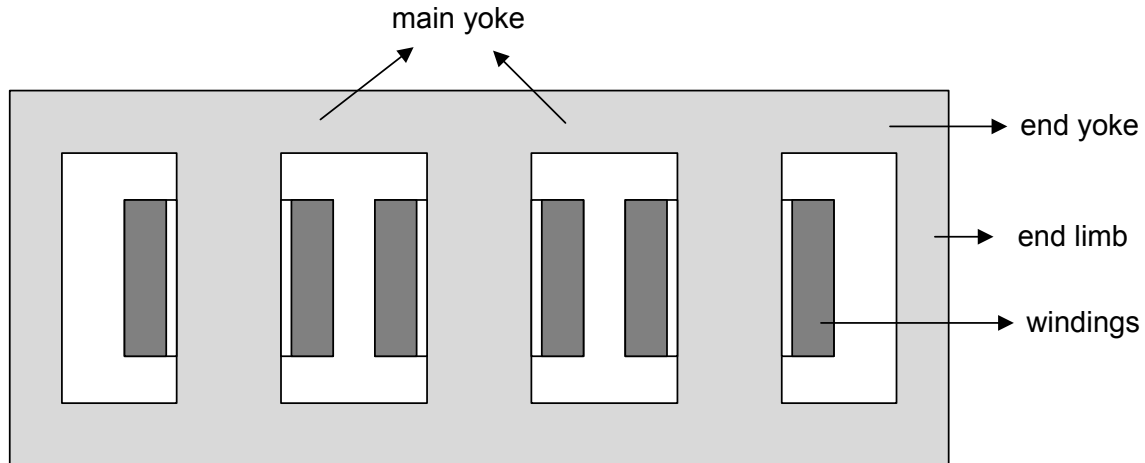


Figure 1: Schematic picture of a three phase three limb transformer.

An ordinary three phase three limb transformer is magnetically asymmetric. The center phase has a magnetic path which is shorter than the paths of the two outer phases. This causes inequality of phase magnetizing current and a shift in phase position from the symmetrical positions [10]. This also results in unequal no-load currents and losses.

### 2.2. Three Phase Five Limb Transformer

Another arrangement of core limbs is 'three phase five limb transformer' which is mainly used as generator step-up and as an inter-bus transformer (for connecting two buses) [11]. The five limb transformer has two additional limbs whose area is almost half as compared to the main limb area. Figure 2 shows a general core construction diagram.



**Figure 2: Schematic picture of a three phase five limb transformer.**

The magnetic length represented by the end limb and end yoke has a higher reluctance as compared to the one presented by the main yoke. The presence of two additional limbs, one on either side serve to provide flux return path external to the wound limbs which allows the yoke depth to be reduced [9]. Hence, larger power transformers with lower heights can be manufactured which facilitate easier land transportation.

### **2.3. Open Circuit Zero Sequence Impedance**

For a three phase transformer, the positive and negative sequence impedance values are identical but the zero-sequence impedance depends considerably on the construction of the transformer.

#### **2.3.1. Three Phase Three Limb Transformer**

Most of the small and medium sized transformers are three phase three limb transformers with core type construction. As explained earlier, it has three limbs that serve as magnetic flux path. Under balanced conditions, the three phases have their three respective currents which are displaced  $120^\circ$  from each other. Accordingly, the flux vectors in three phases are displaced  $120^\circ$  apart and it is summed to zero in the yoke. This condition is true when the supply voltage is balanced and hence residual flux (i.e. the sum all the three phases) is zero [12].

The flux leakage passes from the top yoke through the high reluctance air gap and into the tank. In this case, the tank acts as an equivalent delta winding. The tank influences the zero-sequence reactance in the following way. It provides a comparatively lower reluctance path (as compared to air) to the zero-sequence flux which has an effect of increasing the reactance. But, the tank is also enclosing the three phases and it acts as a short circuit winding which reduces the reactance. The latter effect is more dominant and hence the zero-sequence reactance inside the tank is appreciably less than that without it. [13]. For three limb designs without a stabilizing delta winding, the tank is the deciding factor and the typical value for zero-sequence impedance is between 75 – 200 % of the positive-sequence impedance value [14].

### **2.3.2. Three Phase Five Limb Transformer**

In case of a three phase five limb transformer, the flux has a return path through the end yokes and hence the zero-sequence magnetizing reactance is substantially close to the positive-sequence magnetizing reactance (quite a high value) unless the voltage applied is such that the yokes and end limbs saturate. For an applied voltage of zero-sequence close to the rated voltage, the yokes and end limbs will get completely saturated which results in a lower value of magnetizing zero-sequence voltage, close to that of a transformer with a three phase three limb core [13].

## **2.4. Transformer Losses**

Transformer losses are divided into losses in the windings, termed as 'copper loss', and those in the magnetic circuit, termed 'iron loss'. These losses vary with load current and may be classified as 'no-load' or 'full-load' losses. Winding resistance dominates the full load losses whereas hysteresis and eddy currents contribute to over 99% of no-load losses [15].

### **2.4.1. Eddy Currents Loss**

The core of a transformer is built by thin laminated sheets of ferromagnetic material. These sheets can be seen as a single short circuited loop through its entire length. Alternating flux in the core induces small amounts of circulating currents namely Eddy currents [16]. The Eddy currents circulate within the core and are responsible for resistive heating of the core. It is proportional to the square of supply frequency; however this is only true for low frequencies.

Eddy current loss can be minimized by reducing the thickness of lamination and increasing the resistivity of the material in order to make it less easy for Eddy currents to flow [15].

### **2.4.2. Hysteresis Loss**

The hysteresis loss is proportional to the area of the hysteresis loop (Figure 3) and supply frequency since one period of current represents one lap around the hysteresis loop. The hysteresis loop is a characteristic of the material and is a function of peak flux density [15]. It also depicts the effect of saturation i.e. after a certain value of flux; it cannot be increased any further, even if the current keeps on increasing. Consider Figure 3 for hysteresis loss:

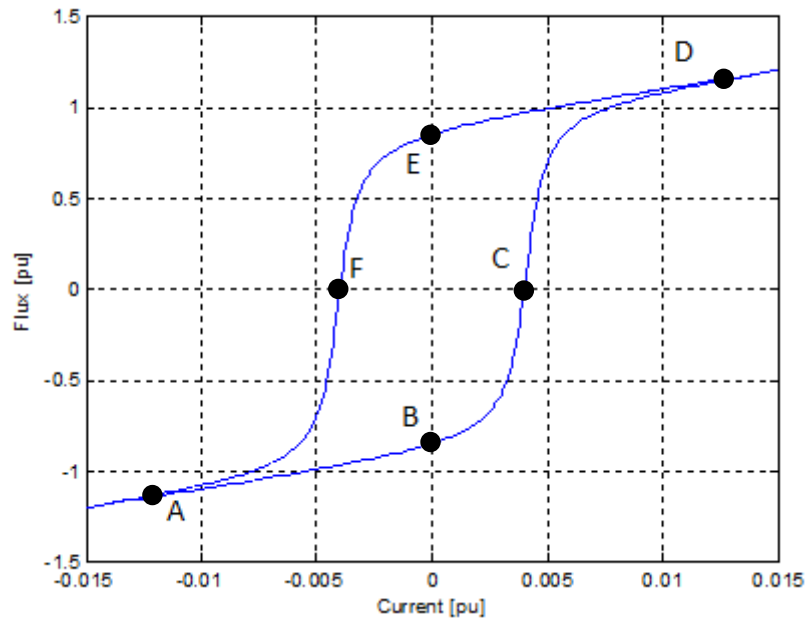


Figure 3: Hysteresis loop of a ferrite material with flux plotted versus magnetizing current.

Consider 'A' as starting point where both the flux and magnetizing current have their maximum negative value. As the current decreases to zero (point 'B') there will still be a remanent flux in the core. When moving towards further positive values of the current, the flux increases and at point 'C' the flux in the core is zero even if a current is flowing. This occurs since not all of the magnetic domains have the same directions within the material. When the magnetizing current reaches its peak value at point 'D', all the magnetic domains have aligned and the rapid increase in flux has been slowed down. As the current derivative becomes negative the cycle goes back to point 'E' where the current is again zero and the remanent flux is in the opposite direction compared to point 'B'. Further increase of current in the negative area causes the flux to change direction and move via point 'F' to point 'A' and one period of the current is completed ([16] and [17]). Hysteresis loss can be minimized by using a material with minimum hysteresis loop [15].

### 2.4.3. Winding Loss

Winding loss constitutes the  $I^2R$  losses and the leakage reactance. The leakage reactance appears due to the fact that all the flux produced by the primary winding is not linked to the secondary winding. By increasing the conductor cross sectional area, resistance is reduced and hence the losses are decreased [17].

### 3. Case Set-Up

#### 3.1. Voltage Profiles

A total of four different voltage profiles were studied which are shown in the following figures [18]:

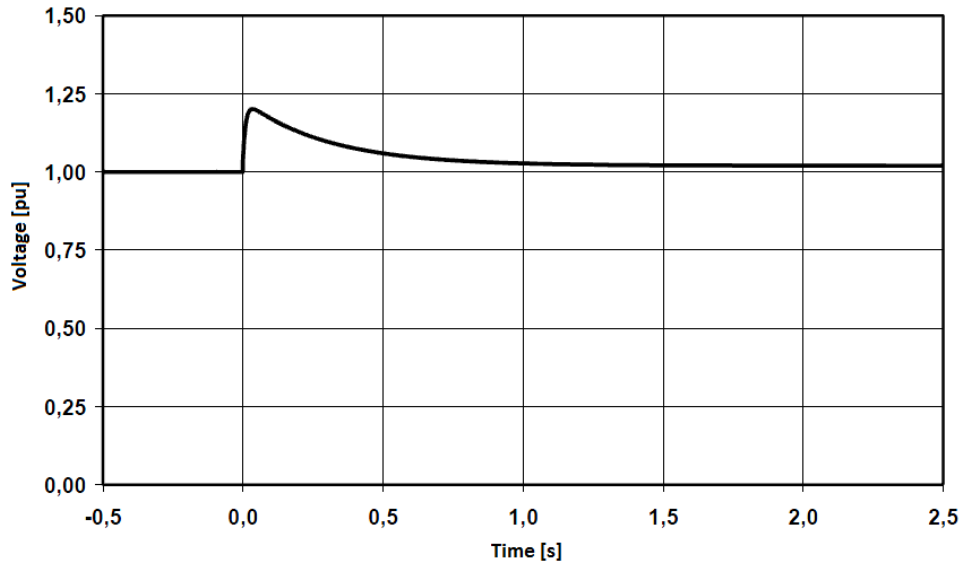


**Figure 4: Load rejection at full power and changeover to in-house turbine with functional voltage regulator.**

Figure 4 shows a voltage profile that represents a loss of load that is followed by transition to the in-house turbine with a functional automatic voltage regulator (AVR). The profile is constructed by three factors i.e. previous faults, the function of magnetizing control and simulation of load rejection performed by OKG AB [18].

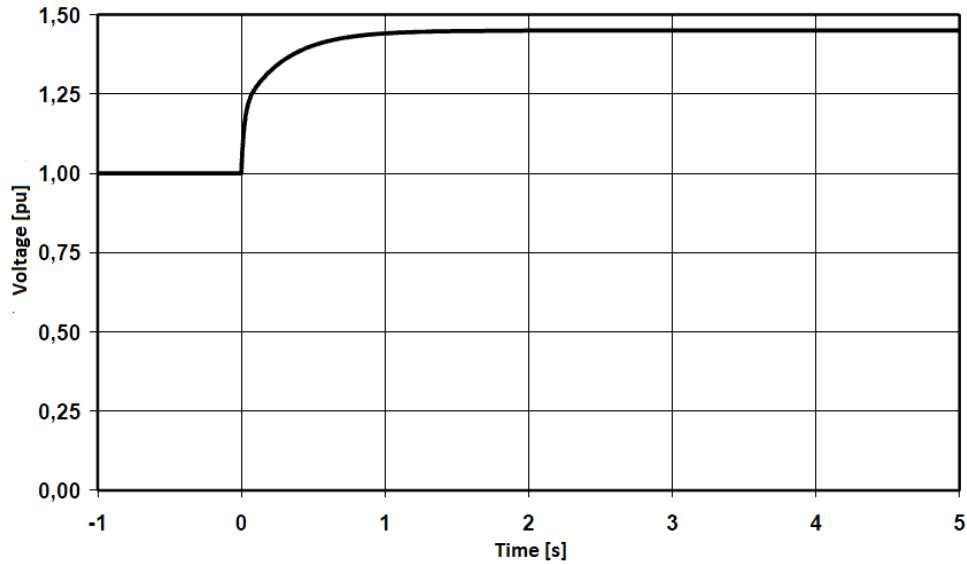


Figure 5: Load rejection and changeover to in-house turbine with field current regulation.

Figure 5 shows a voltage profile of load rejection while the generator was operating in field current regulator mode. The time until reaching a stable voltage level is dependent on the peak voltage factor and the parameters of the field current regulator [18].

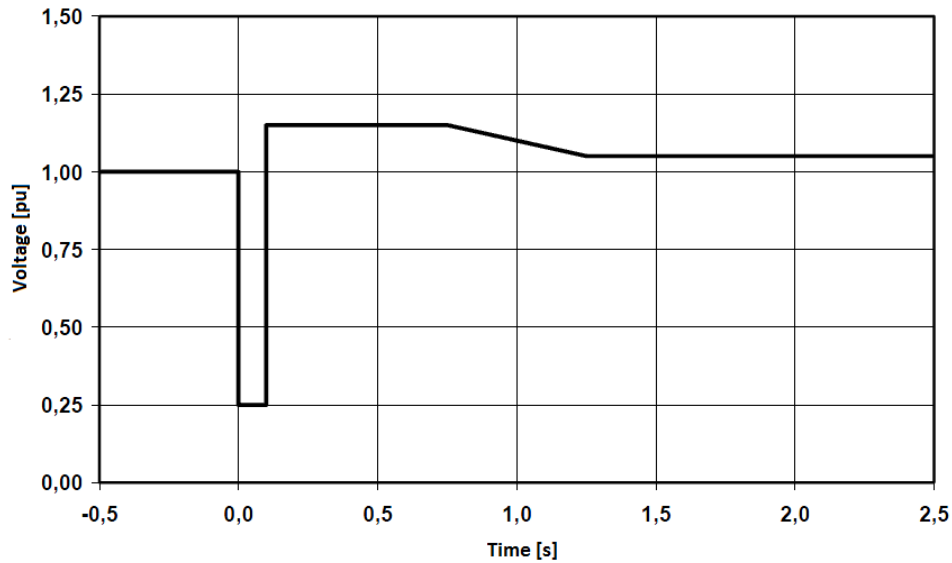


Figure 6: Fault disconnection and changeover to in-house turbine, dip time 100 ms.

Figure 6 shows a profile of a three phase bus bar fault of 100 ms with a post-fault voltage level is 1.15 pu. The fault is expected to trip and the supply is switched over to the in-house turbine resulting in a slight overvoltage which is regulated in an ordinary manner [18].

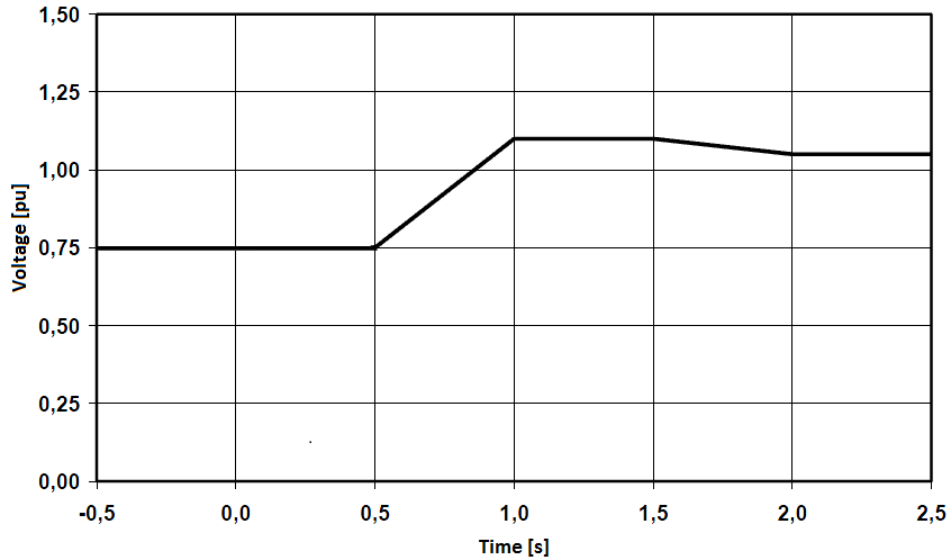


Figure 7: Alternate swell, as a combination of low initial voltage converting after an expected fault into a swell and then switch to in-house turbine.

Figure 7 shows an adapted voltage profile that is meant to show the differences in behavior during less abrupt swells. The profile starts at a voltage of 0.75 pu which means a low flux in the transformer; which is then followed by a gradual overvoltage. This profile was an updated version profile 7 in [18].

### 3.2. Description of Transformers

The transformers were manufactured by Noratel AB, rated to 4 kVA each with 100 % extra insulation and 40 % extra copper area to reduce the R/X ratio of small transformers making it more comparable to larger transformers. The transformers were modified with a connection plate to simplify the connections and reduce the risk of faulty and unsafe operation. The transformers are shown in Figure 8 and Figure 9 below. The transformer parameters and their rating plates can be found in Appendix A.



Figure 9: The five limb transformer.



Figure 8: The three limb transformer.

### 3.3. Determination of Transformer Parameters

In order to model the transformers accurately, several parameters were extracted practically. These parameters are then used in the models to perform analysis and comparison. This helped to establish differences between the three limb and five limb transformers.

#### 3.3.1. Open Circuit and Short Circuit Test

For a non-ideal model (Figure 10), it is required to perform an open circuit and a short circuit test on the transformer which gives information about the following parameters:

$R_p$ : The resistive component in the primary winding.

$R_s$ : The resistive component in the secondary winding.

$L_{p\lambda}$ : The primary leakage inductance, representing the flux that flows outside the magnetic core path.

$L_{s\lambda}$ : The secondary leakage inductance, representing the flux that flows outside the magnetic core path.

$L_m$ : Magnetizing inductance that represents the finite permeability of the core.

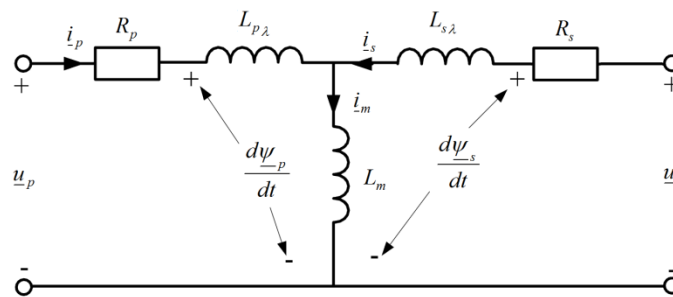


Figure 10: Transformer equivalent circuit.

In Figure 10 the  $p$  and  $s$  denotes the primary and secondary values respectively. The open circuit test is performed with the secondary side as open (Figure 11). This means that the current will only flow in the primary side of the transformer.  $R_p$  and  $L_{p\lambda}$  are very small in comparison to  $L_m$  and can therefore be neglected due to their small voltage drop. The test is performed by increasing the primary voltage to its rated value and measuring the current flowing in the loop and open circuit power. These are then used to calculate the parameters of the parallel branch. In many models there is a resistive component added in parallel with the magnetizing inductance, in order to represent the iron losses.

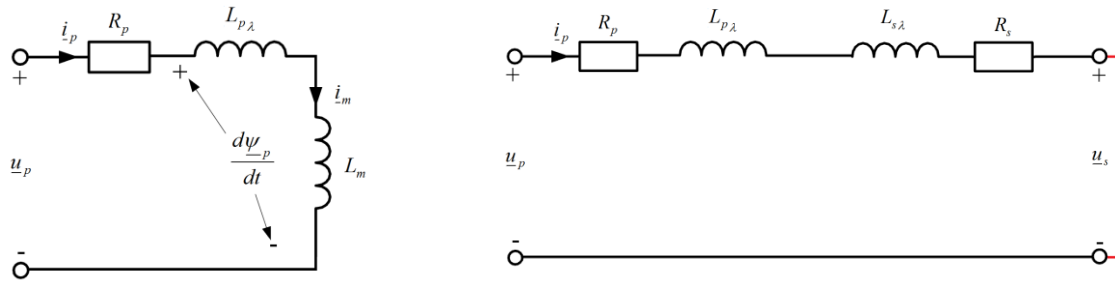


Figure 11: To the left; Equivalent circuit during open circuit test. To the right; Equivalent circuit for short circuit test.

The short circuit test is performed with the secondary terminal short circuited. The Primary voltage is increased until the rated current is reached in the primary winding, since the turns ratio used is 1:1, while power and current is measured. This voltage is significantly lower than the rated voltage of the transformer [19]. The equations and the measurement setup for the two tests can be found in Appendix A.

### 3.3.2. Magnetizing Inductance Test

To acquire a more specific representation of  $L_m$ , an open circuit test was performed (Figure 11). The voltage was varied in small steps and the open circuit current was measured. These were later used to plot  $L_m$ 's dependence on the open circuit current i.e. the magnetizing current. The obtained curve was used to depict the saturation in the MATLAB model. The measurements are presented in Appendix A and a plot of  $L_m$  is presented in Figure 14.

### 3.4. Determination of Loads

Two separate loads were used in the experiments namely resistive and inductive load which were both delta connected. All four voltage profiles were applied at the following percentage loadings of respective loads:

Table 1: Loading Percentage.

Resistive Load		Inductive Load	
%	$\Omega$ /phase	%	$\Omega$ /phase
50	120	10	448
75	81	20	230
100	62	40	115

#### 3.4.1. Calculation for Loads

The available resistive as well as the inductive load had a rating of  $3 \times 220 V_{L,RMS}$  in delta connection. The resistive box (Figure 12) has ten while the inductive box (Figure 13) has 11 variable steps which correspond to different values of resistance and inductance. The desired step is chosen accordingly as per the calculations.

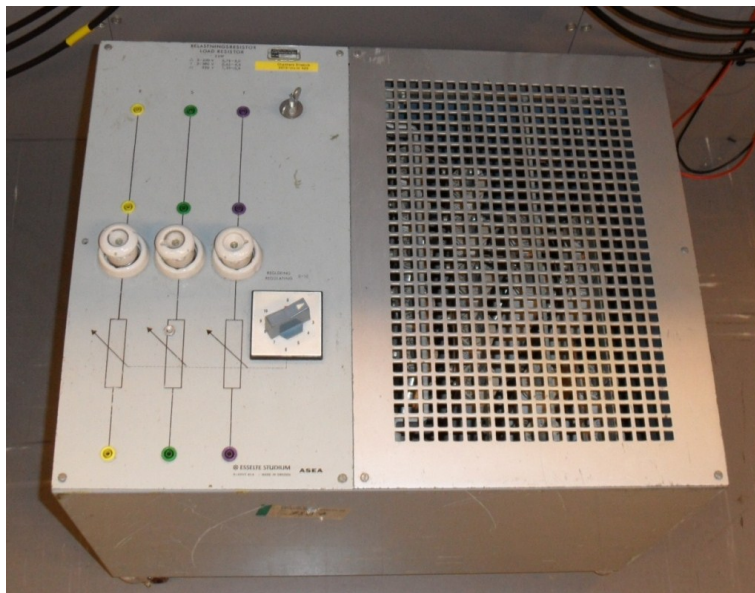
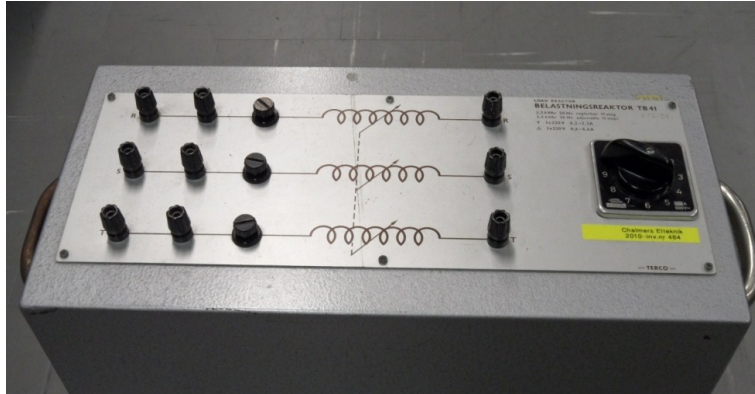


Figure 12: Resistive Load.



**Figure 13: Inductive Load.**

The calculations for selection of load are done and the nearest value of resistance that will load the transformer to approximately the desired value is chosen. Since the rating of the transformer is 4 kVA with 200 V<sub>L-L,RMS</sub>; this implies a rated current of 5.79 A at full loading. Table 2 shows that for a loading of 50%, the desired current is 2.89 A. However, due to the limitation of step variation of the resistor box, we can achieve 2.75 A at step number 4. The same procedure follows for the other loadings.

**Table 2: Percentage of loading and step numbers.**

	<b>% Loading</b>	<b>Desired Current [A]</b>	<b>Available Current [A]</b>	<b>Step #</b>
<b>Inductive</b>	10	0.579	0.49	1
	20	1.158	1.176	2
	40	2.31	2.13	4
<b>Resistive</b>	50	2.89	2.75	4
	75	4.34	4.10	6
	100	5.79	5.34	8

### 3.5. Model

Two models were derived from earlier machine models which provided good accuracy on dynamic and transient studies ([20] and [21]). These rotating models were made non-rotating and the extracted parameters (see Chapter 3.3) were implemented. The models can then be compared to the actual result from experimentation (see Chapter 4.2).

#### 3.5.1. Park Model Transformer Model

Based on the fifth-order park model which is also referred to as the two-axis model [20], the main equations are;

$$u_p = i_p R_p + \frac{d\psi_p}{dt} + j\omega_k \psi_p \quad (3.1)$$

$$u_s = i_s R_s + \frac{d\psi_s}{dt} + j\omega_k \psi_s \quad (3.2)$$

$$\psi_p = L_p i_p + L_m i_s = (L_{p\lambda} + L_m) i_p + L_m i_s \quad (3.3)$$

$$\psi_s = L_m i_p + L_s i_s = (L_{s\lambda} + L_m) i_s + L_m i_p \quad (3.4)$$

where,  $p$  and  $s$  denotes the primary and secondary and  $\omega_k$  denotes the angular speed of the coordinate system. Since the model is implemented in alpha-beta coordinated system, therefore  $\omega_k=0$ . These equations can be expressed in matrix form:

$$\mathbf{U} = \mathbf{R}\mathbf{I} + \mathbf{L} \frac{d\mathbf{I}}{dt} \quad (3.5)$$

Where,  $\mathbf{U}$  is the voltage vector,  $\mathbf{I}$  is the current vector,  $\mathbf{R}$  is the resistance matrix and  $\mathbf{L}$  is the inductance matrix.

$$\mathbf{U} = \begin{bmatrix} u_{p\alpha} \\ u_{p\beta} \\ u_{s\alpha} \\ u_{s\beta} \end{bmatrix} \quad \mathbf{I} = \begin{bmatrix} i_{p\alpha} \\ i_{p\beta} \\ i_{s\alpha} \\ i_{s\beta} \end{bmatrix} \quad \mathbf{L} = \begin{bmatrix} L_p & 0 & L_m & 0 \\ 0 & L_p & 0 & L_m \\ L_m & 0 & L_s & 0 \\ 0 & L_m & 0 & L_s \end{bmatrix} \quad \mathbf{R} = \begin{bmatrix} R_p & -\omega L_p & 0 & -\omega L_m \\ \omega L_p & R_p & \omega L_m & 0 \\ 0 & -\omega L_m & R_s & -\omega L_s \\ \omega L_m & 0 & \omega L_s & R_s \end{bmatrix} \quad (3.6)$$

### 3.5.2. Three Phase Transformer Model

This model is based on the three phase machine model presented in [21]. It is then modified to a transformer model by removing the rotating behavior and the main equations become:

$$[U] = [R][I] + \frac{d}{dt}([L][I]) \quad (3.7)$$

This becomes

$$[U] = [R'][I] + [L] \frac{d}{dt}([I]) \quad (3.8)$$

where

$$[R'] = [R] + \frac{d}{dt}[L], \quad (3.9)$$

This is made to get the equations onto the form of state space equations shown in 3.13 and 3.14.

The voltage and current vectors are;

$$[U] = \begin{bmatrix} u_r \\ u_s \\ u_t \\ u_u \\ u_v \\ u_w \end{bmatrix} \quad [I] = \begin{bmatrix} i_r \\ i_s \\ i_t \\ i_u \\ i_v \\ i_w \end{bmatrix}, \quad (3.10)$$

while the resistance and inductance matrixes have been derived for non-rotating model and are;

$$[R'] = \begin{bmatrix} R_p & 0 & 0 & 0 & 0 & 0 \\ 0 & R_p & 0 & 0 & 0 & 0 \\ 0 & 0 & R_p & 0 & 0 & 0 \\ 0 & 0 & 0 & R_s & 0 & 0 \\ 0 & 0 & 0 & 0 & R_s & 0 \\ 0 & 0 & 0 & 0 & 0 & R_s \end{bmatrix} \quad [L] = \begin{bmatrix} L_p + M & -M/2 & -M/2 & M & M & M \\ -M/2 & L_p + M & -M/2 & M & M & M \\ -M/2 & -M/2 & L_p + M & M & M & M \\ M & M & M & L_s + M & -M/2 & -M/2 \\ M & M & M & -M/2 & L_s + M & -M/2 \\ M & M & M & -M/2 & -M/2 & L_s + M \end{bmatrix} \quad (3.11)$$

where

$$M = \frac{2 X_m}{3 2\pi f}. \quad (3.12)$$

### 3.5.3. Implementation in MATLAB

The two models discussed both have several differential equations that need to be solved. This is done by using the following state space equations,

$$\frac{dx}{dt} = Ax + Bu \quad (3.13)$$

$$y = Cx + Du \quad (3.14)$$

where, x is the state vector, u is the input vector and y is the output vector. A, B, C and D are state-space matrices that express the dynamics of the system to be simulated [22].

### 3.5.4. Saturation Modeling

After taking the measured values of  $L_m$  as a function of  $i_m$ , the curve was fitted to obtain an equation. This ensured that each individual value of magnetizing current corresponds to a new value of  $L_m$ .

The equations for two different cases of magnetizing current are as follows:

For low magnetizing current the value of  $L_m$  is the result of (3.15), that is when the derivative of the magnetizing inductance with respect to the magnetizing current is positive in Figure 14. This gives the V-I-characteristics in Figure 15,

$$L_m = ki_m \quad (3.15)$$

When the magnetizing current is above the peak of the magnetizing inductance, (3.16) is the function;

$$L_m = \frac{p}{(i_m+q)} \quad (3.16)$$

The values of constants p, q and k are shown in Table 3.

**Table 3: Values of constants for (3.15) and (3.16).**

Type	$p$	$q$	$i_m \text{ peak}$	$k$
3 limb	0.4751	0.2405	0.13	9.31
5 limb	0.5395	0.2754	0.1498	8.31

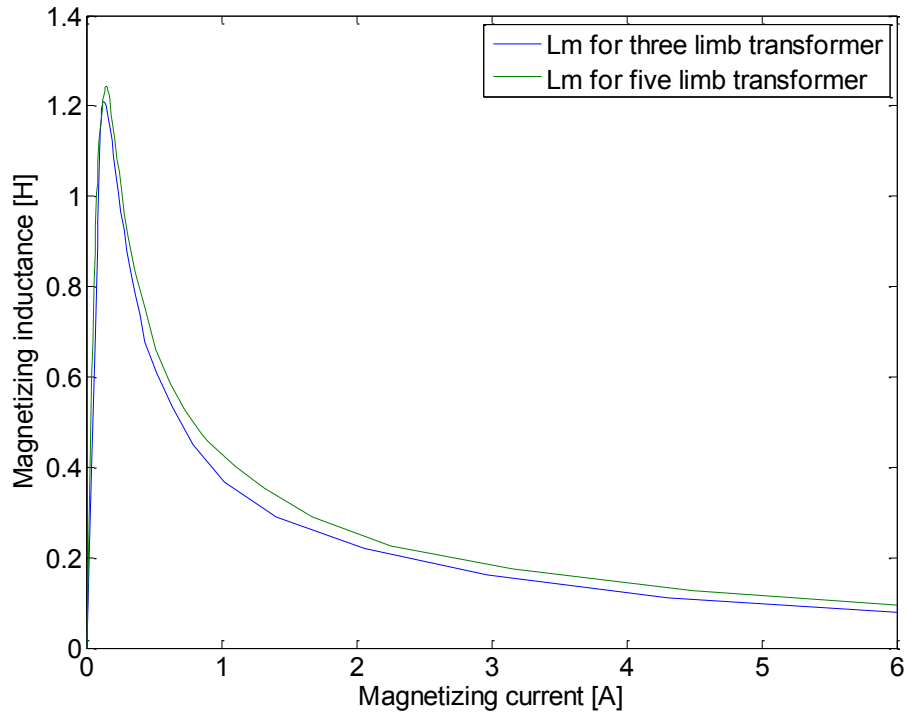


Figure 14: Plot used for the modeling of saturation obtained during the open circuit test.

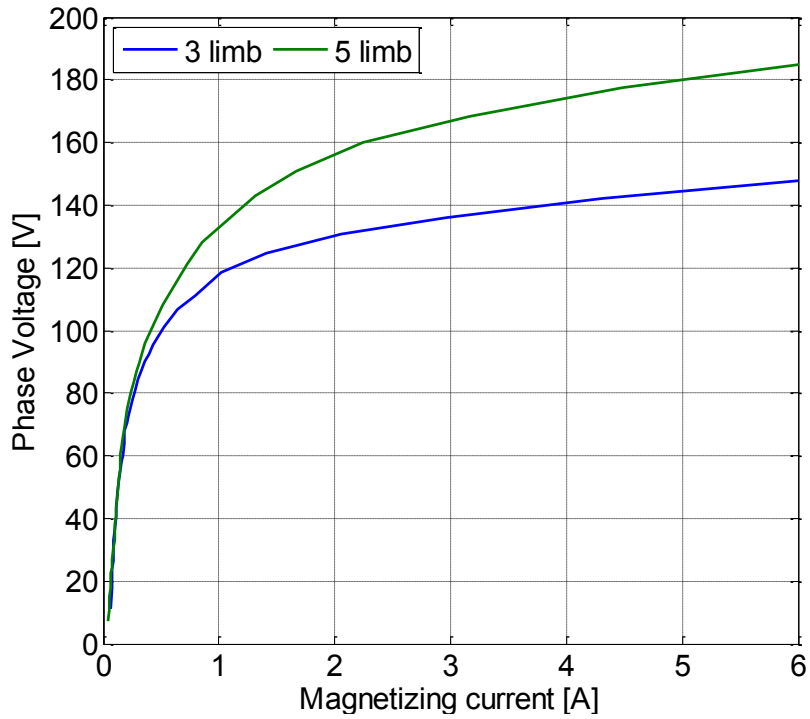


Figure 15: V-I characteristics obtained during open circuit test, see Appendix A.

### 3.6. Laboratory Set Up

Verification of simulation results was done in a laboratory set-up in which a three phase three limb and three phase five limb transformer were used. Both these transformers had a rating of 4 kVA having the possibility of being connected in wye or delta connection. The general schematic of the set-up is shown in Figure 16.

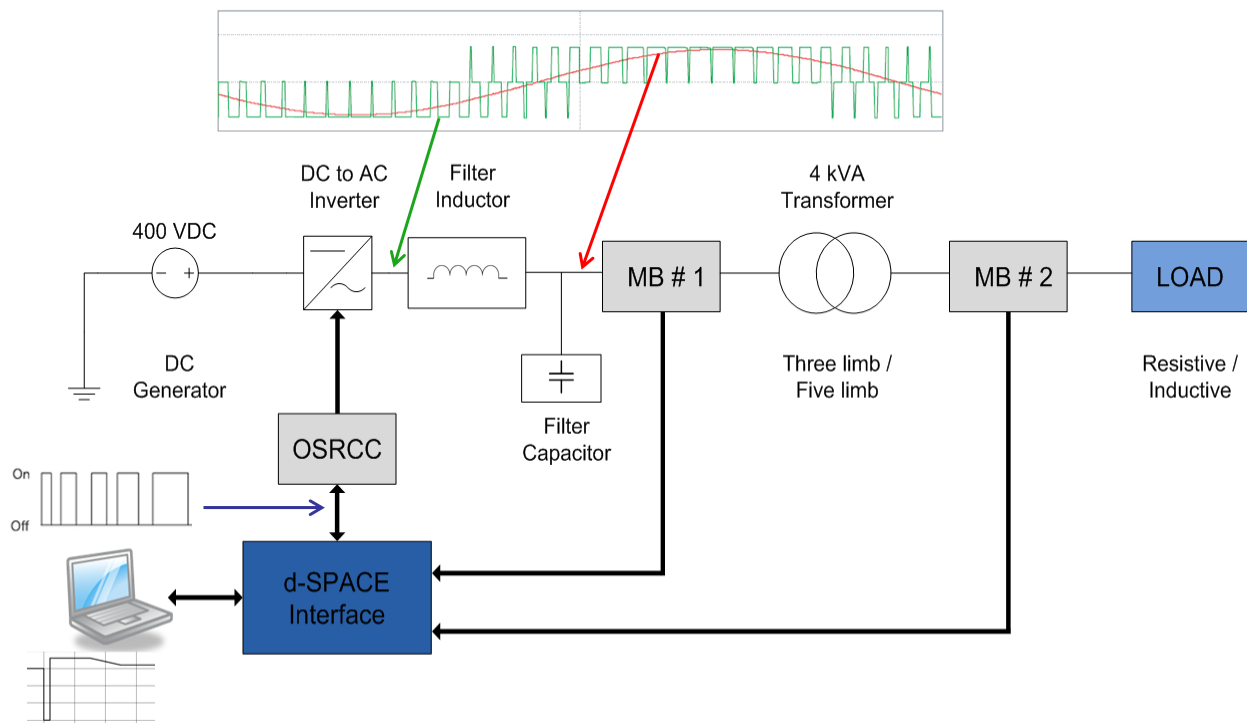


Figure 16: Laboratory Set-up.

A DC / AC inverter is fed by a DC generator that is connected to the test transformer via a filter inductor and a filter capacitor which then feeds the load. It is to be noted that the output of the converter is not perfectly sinusoidal, so a suitable sized filter inductor and capacitor is connected at the output of the converter before feeding the transformers. Since the filter inductor are in series with the output of the converter; its size had to be chosen in such a manner that it doesn't affect the overall readings. Besides this, the filter capacitor is connected in wye configuration at the output of the inverter. Suitable rated fuses and circuit breakers had been used in the set-up for protection of equipment and personnel.

The voltage dips are implemented in MATLAB using look-up tables. The computer contains an open loop controller created in Simulink by Dr. Massimo Bongiorno, Chalmers University of Technology. In the controller, reference signals of chosen voltage dips are created and compared to a PWM signal [23]. This generates duty cycles for the valves in the inverter which are fed to the gate control circuitry via a real time interface (RTI) called d-SPACE. The signals from d-SPACE are converted to optical signals using an Opto Sending and Receiving Conversion Card (OSRCC) and then they are routed to the gate control

circuitry. Current and voltage are measured at the primary and the secondary of the transformer with the help of measurement box (MB) and the data is then sent to the data acquisition computer via the RTI. Figure 17 shows a glimpse of the laboratory set-up where one can see the test circuit components from the inverter to the transformer.

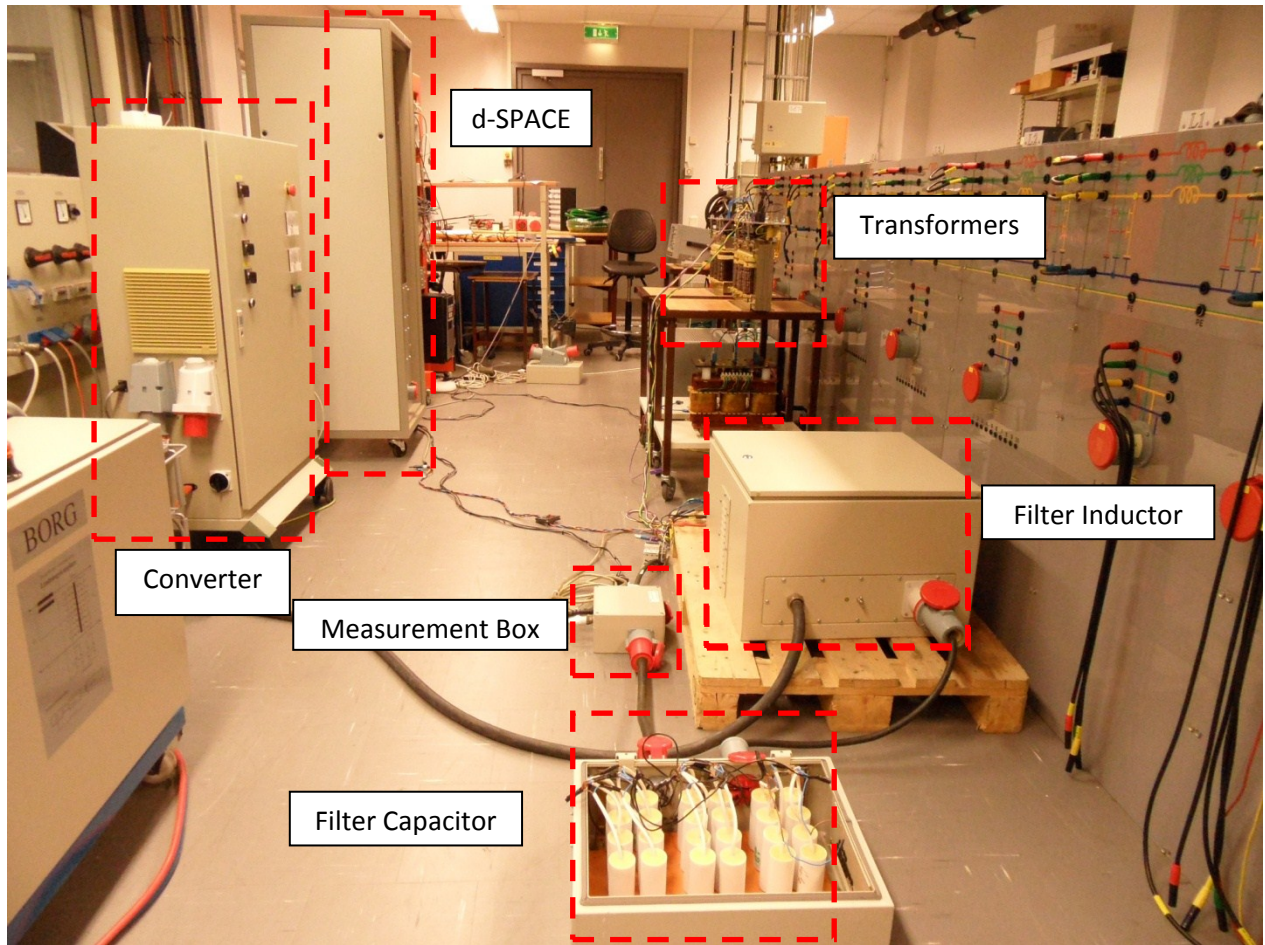


Figure 17: Picture from the lab setup.

### 3.6.1. Real-Time Interface: d-SPACE

d-SPACE is the RTI between the software (MATLAB) and the hardware (inverter and test circuitry). It takes PWM signals from MATLAB and sends it on to the OSRCC along with the acquisition of measurement data for further analysis. The following figure shows the front view of the panel including the d-SPACE computer, d-SPACE interface, measurement card # 1 and OSRCC.

A detailed explanation of the connection scheme along with an illustration of parts is shown below:

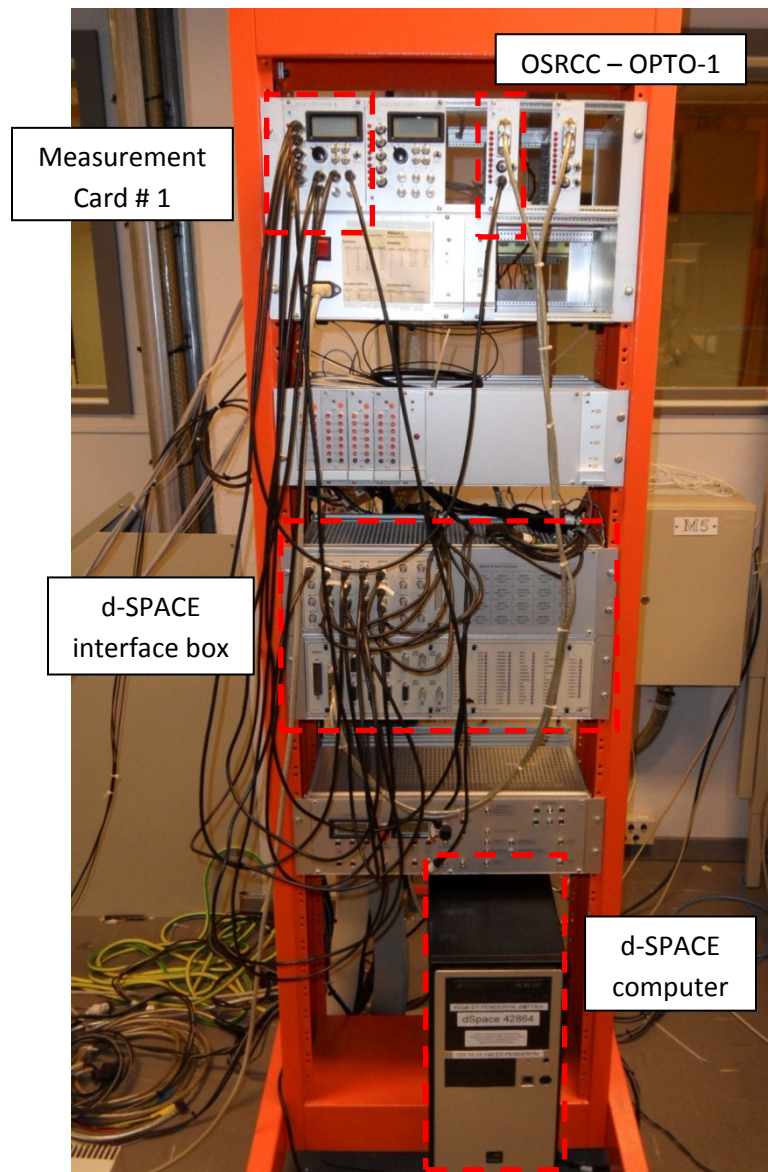


Figure 18: Picture of d-SPACE, measurement card and connections from setup.

### 3.6.1.1. d-SPACE Interface box

The interface box of d-SPACE acquires data signals from the measurement boxes and sends it to the computer system. The set of BNC cables marked **C-1** in Figure 19 contain voltages and currents for the three phases of primary and secondary side of transformer. It also consists of a  $U_{dc}$  signal that is obtained from 'Measurement card # 1'. The cable **C-2** takes the PWM signals from the d-SPACE and sends it to the OSRCC namely to OPTO -1.

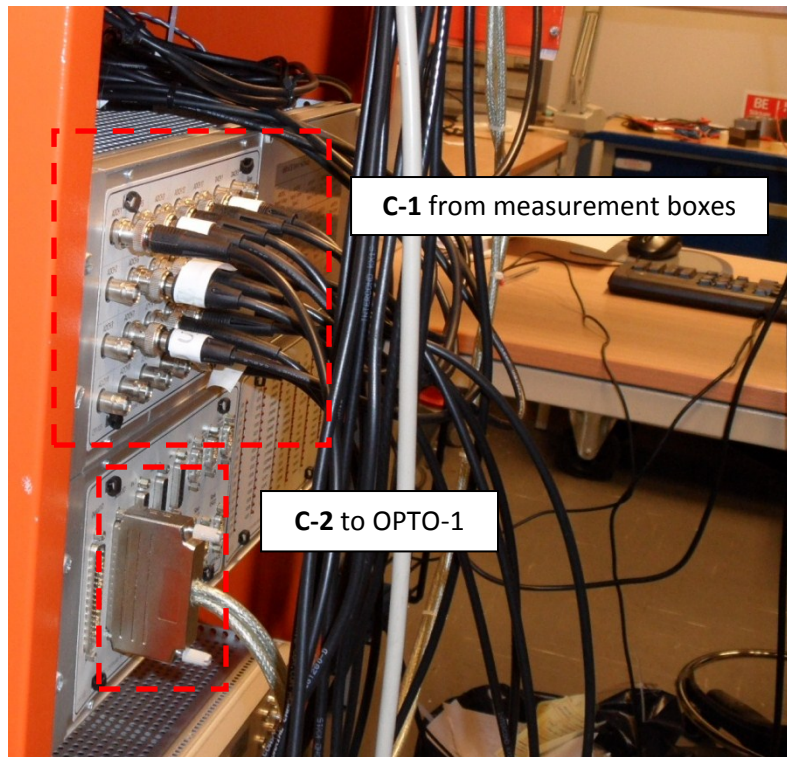


Figure 19: Connections of d-SPACE interface box.

### 3.6.1.2. Measurement card and OSRCC

Figure 20 shows the measurement card and OPTO-1. **C-3** connects external error signals to OPTO-1 to block PWM signals in case of any external errors. The measurement of the  $U_{dc}$  signal i.e. **C-4** is supplied to the RTI box while **C-2** receives the PWM patterns from RTI box. These signals are then converted to optical signals and then sent to the gate control circuitry of the inverter valves.

Figure 21 shows **C-4** which is the output of OPTO-1. Optical signals from OPTO-1 are sent to the gate control circuitry of the inverter while **C-5** gives measurement values of  $U_{dc}$  and  $I_{dc}$  from the inverter.

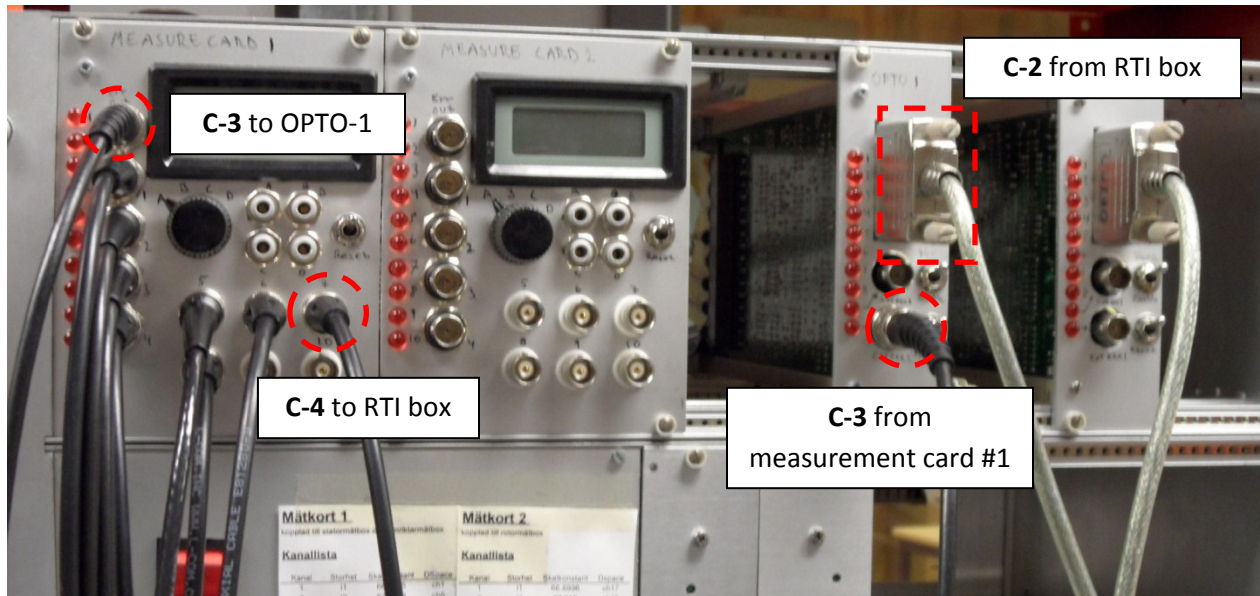


Figure 20: Front view of the measurement card and the signals to the RTI box.

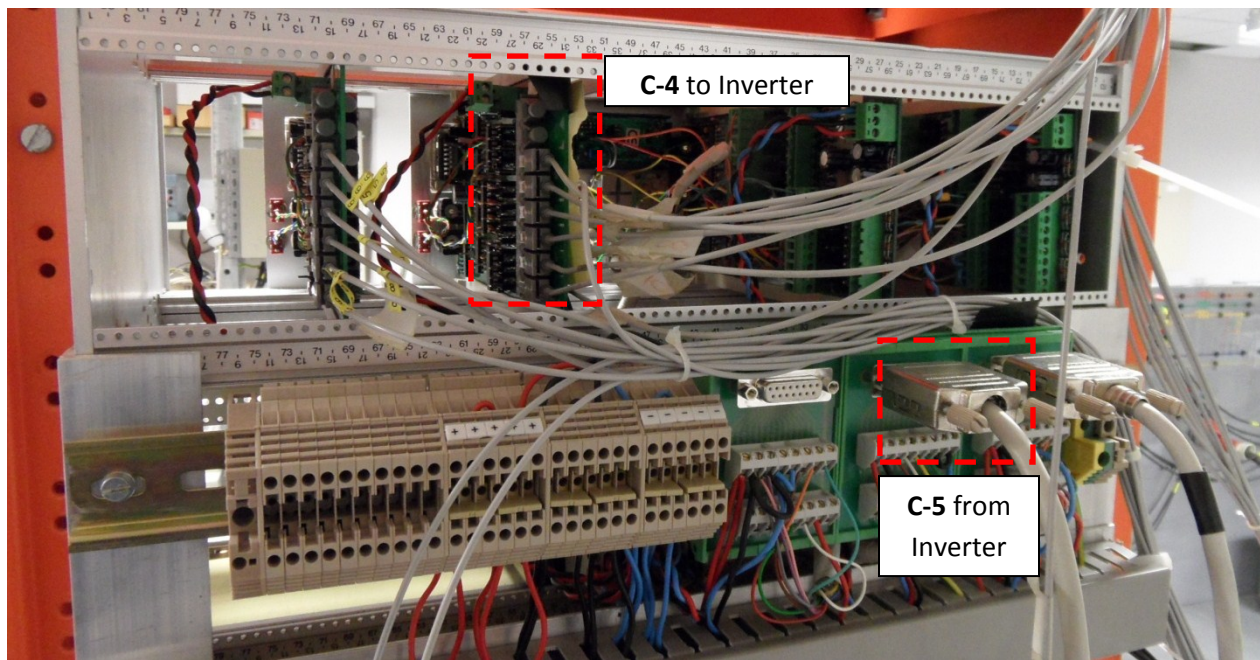


Figure 21: Rear view, displaying the optical fibers to the inverter and the incoming measurements of  $I_{dc}$  and  $U_{dc}$ .

### 3.6.1.3. Measurement Box

The measurement boxes measure the three phase voltages and currents. Two measurement boxes acquire values at the primary and secondary side of the transformer. **C-1** transfers these signals to the RTI box which are then saved in the computer.  $\pm 15 V_{dc}$  is required for the operation of the measurement box itself. Ferrite cores attached to signal cables (not visible in figure) have been used in order to reduce the noise and other disturbances.

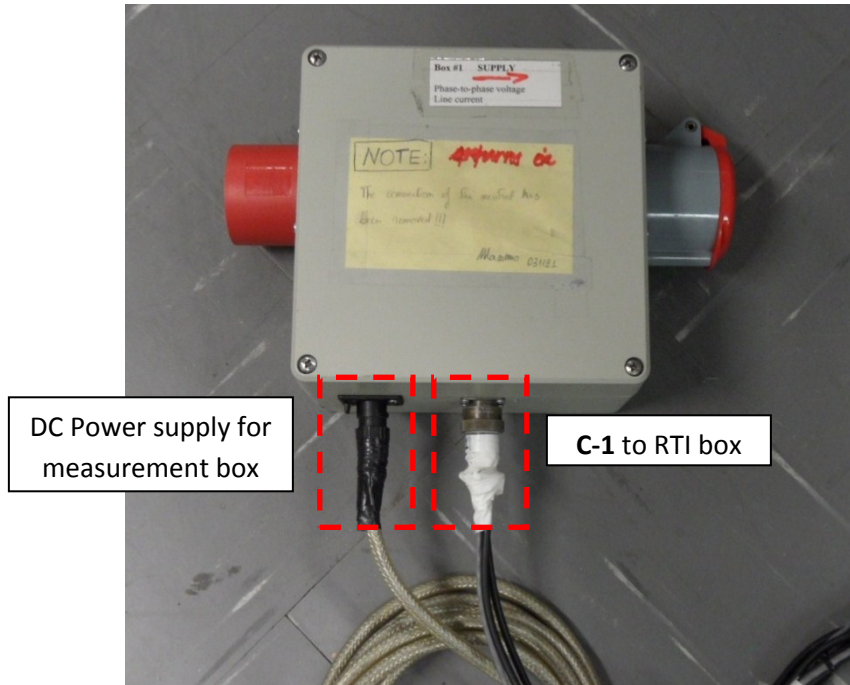


Figure 22: One of the two identical measurement boxes.

### 3.6.1.4. Inverter

Figure 23 shows the inner view of the inverter. **C-4** from OPTO-1 is terminated at the gate control circuitry. **C-5** takes the measurement values of  $U_{dc}$  and  $I_{dc}$  and sends it to measurement card # 1. Figure 24 shows the dc-input to the inverter which in this case was set to  $410 V_{dc}$  along with the three phase output. An auxiliary power of  $230 V_{ac}$  is also required for inverter operation. One can also see the front panel of the inverter in Figure 25.

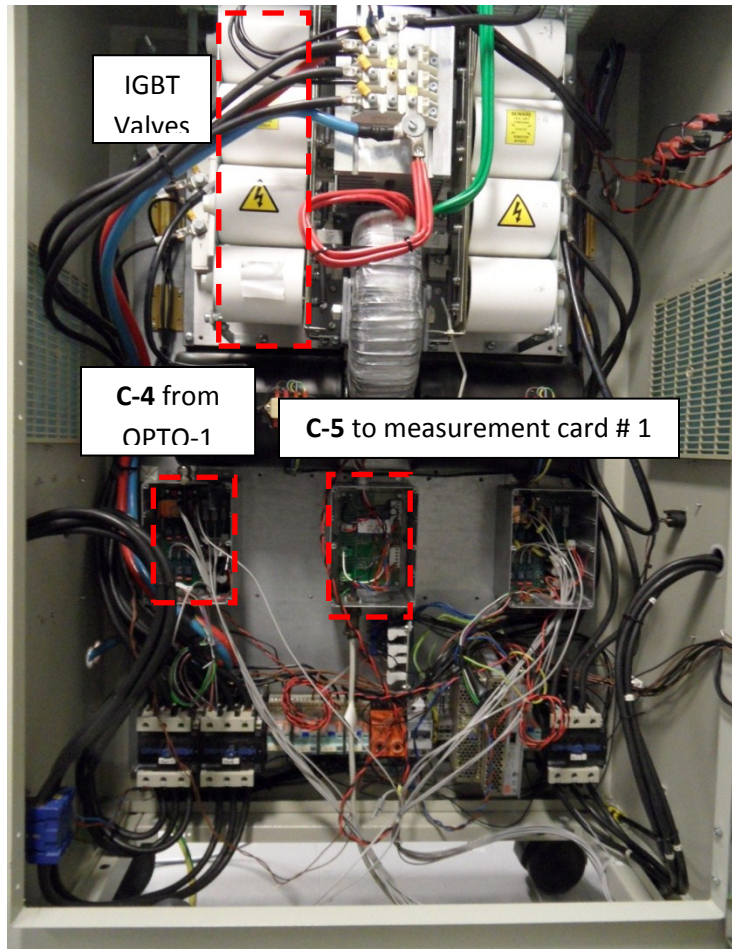


Figure 23: A inner view of the inverter with incoming fibers and cables.

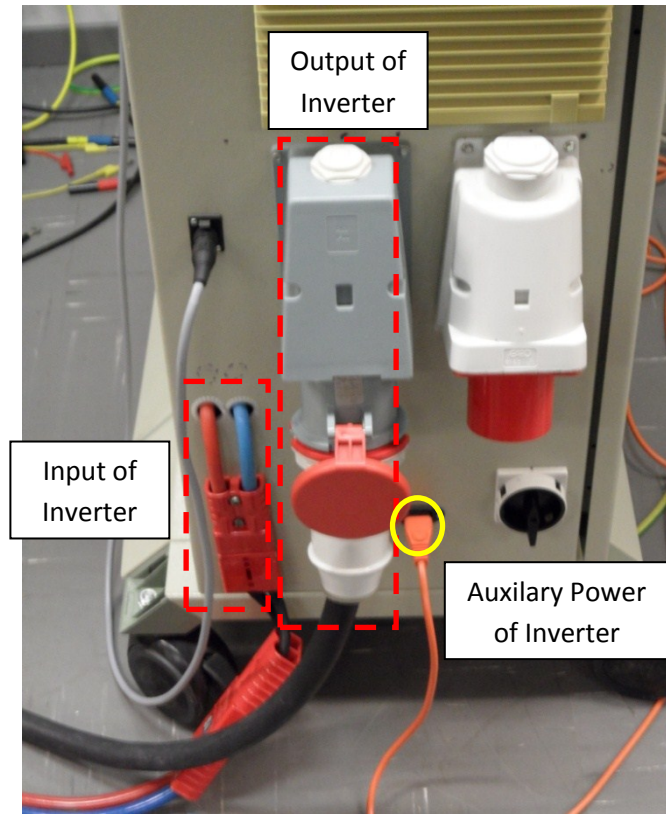


Figure 24: Side view of the inverter showing the auxiliary power, DC-input and the output of the inverter.

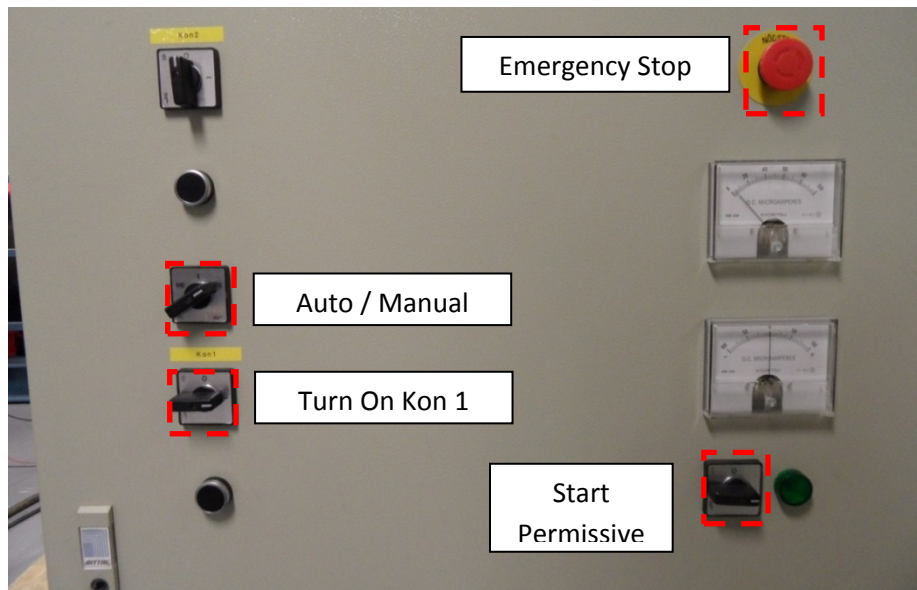


Figure 25: Outer view of the inverter seen from the front panel.

### 3.7. Measurement Accuracy / Errors

All the measurement boxes were checked with the help of an oscilloscope for accuracy and were found to be consistent. This step was repeated to see if the data acquired on the computer was similar to the one measured in the field.

The measurement boxes had current transducers that were rated for 100 A max. Since the current levels in our set-up were much lower than 100 A, a modification was done in order to increase the measurement accuracy. The current transducers had 1 turn which was modified to 4 turns instead. This magnified the measured current by 4 times. It was converted back in the software where the gain of this module was reduced by four times to have a correct reading.

The variance of per phase inductance in the inductive loads constrained that an average value of inductance be calculated to be used further in simulations. Table 4 shows the variation of reactance per phase for the three different loading conditions.

**Table 4: Per phase inductance for the different loading conditions.**

	<b>A-phase reactance (<math>\Omega</math>)</b>	<b>B-phase reactance (<math>\Omega</math>)</b>	<b>C-phase reactance (<math>\Omega</math>)</b>
<b>Stage 1</b>	439	454	452
<b>Stage 2</b>	225	232	231
<b>Stage 4</b>	113	116	116

## 4. Analysis

Analysis was carried out on the secondary voltages of three limb and five limb transformer. The three phase voltages were transformed into the dq coordinate system with all values in pu. This helped to study and compare results in a better way. Figure 26 and Figure 27 shows voltage profile 1 and secondary voltage in abc frame respectively, while Figure 28 shows the same result converted to pu and in the dq coordinate system.

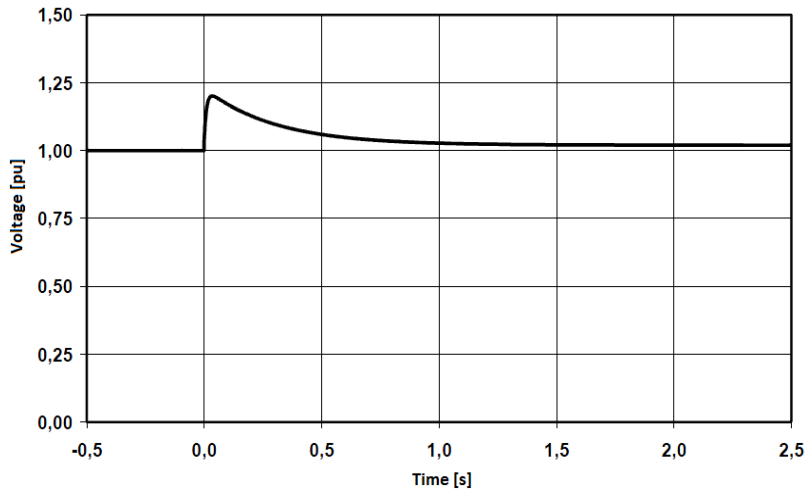


Figure 26: Voltage profile 1 reference in dq components.

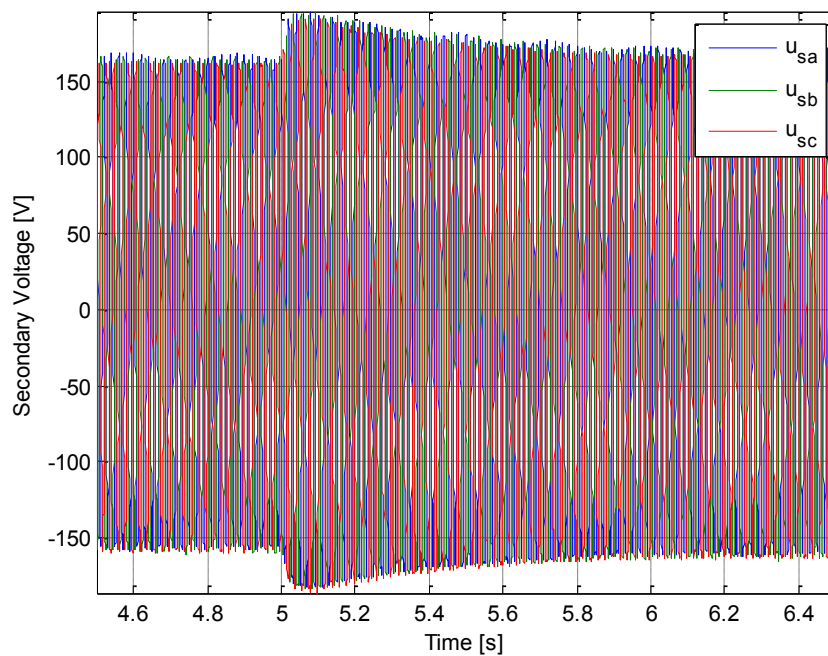


Figure 27: Secondary voltage in abc frame for voltage profile 1.

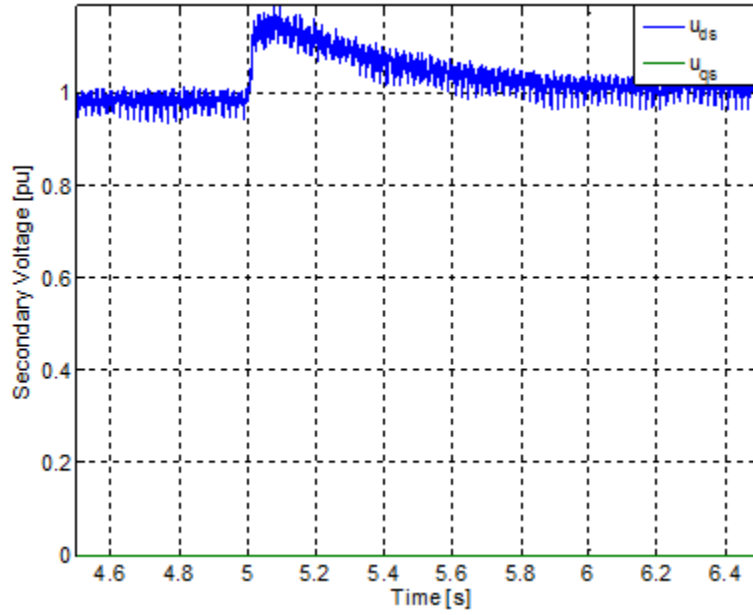


Figure 28: Secondary voltage in pu and dq for voltage profile 1.

#### 4.1. Base Case: Three Phase 3 Limb Transformer

Let us consider the case of three phase 3 limb transformer. Out of the four voltage profiles, profile 2 and 3 will be presented here. The results for the rest of the profiles are presented in Appendix C.

## 4.1.1. Effect of Variation of Load for 3 Limb Transformer

### 4.1.1.1. Voltage Profile 2

Figure 29 shows voltage profile 2. The results of the secondary voltage and secondary current are taken at the instant marked in the Figure 29 which is then plotted in Figure 30 and Figure 31 in the form of a bar plot. This layout is followed throughout the report, since it will provide a better presentation of the results. In the legend, 'u' and 'i' is used for voltage and current respectively while '2' indicates that the value is at the secondary side. The subscript 'three' or 'five' is used for three limb or five limb transformer. Besides this, subscript 'd' or 'q' which are used with the current shows weather the current is in d-axis or q-axis i.e. active and reactive components.

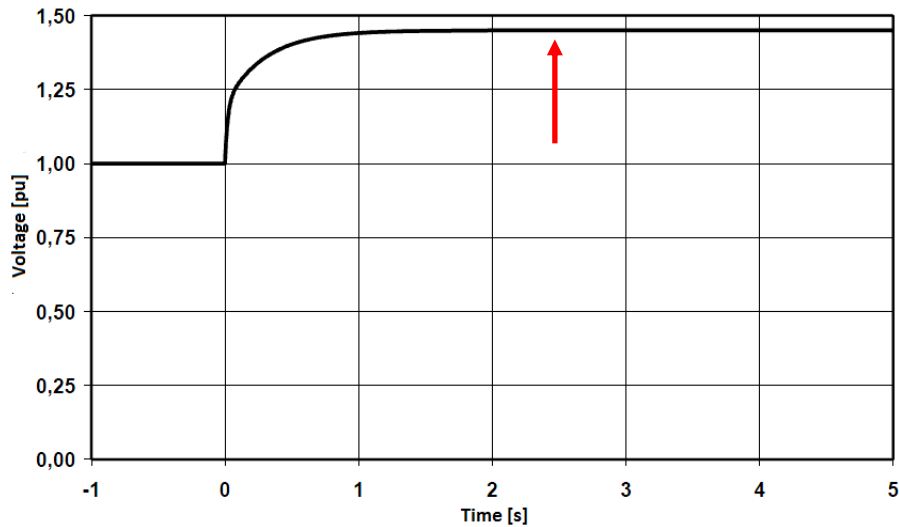


Figure 29: Voltage profile 2 with indication of measurement point.

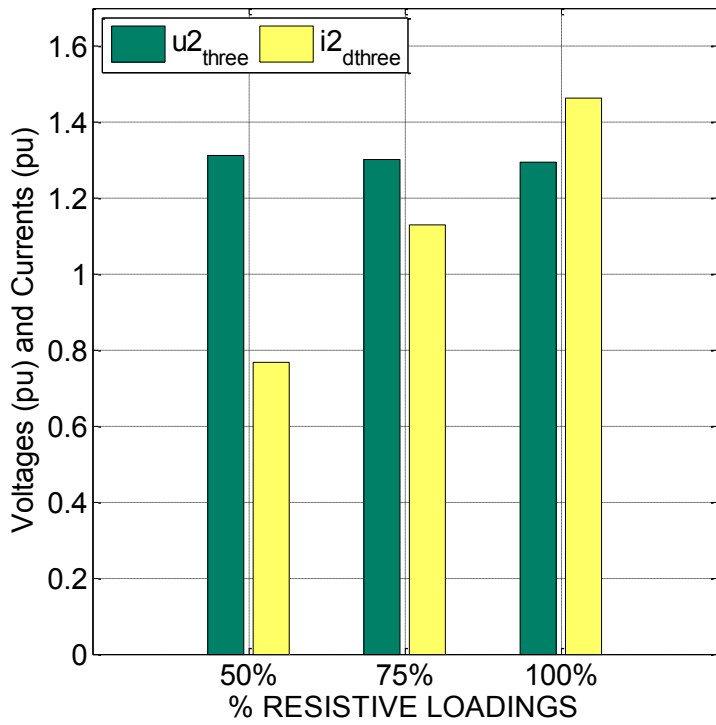


Figure 30: Secondary results for resistive loading.

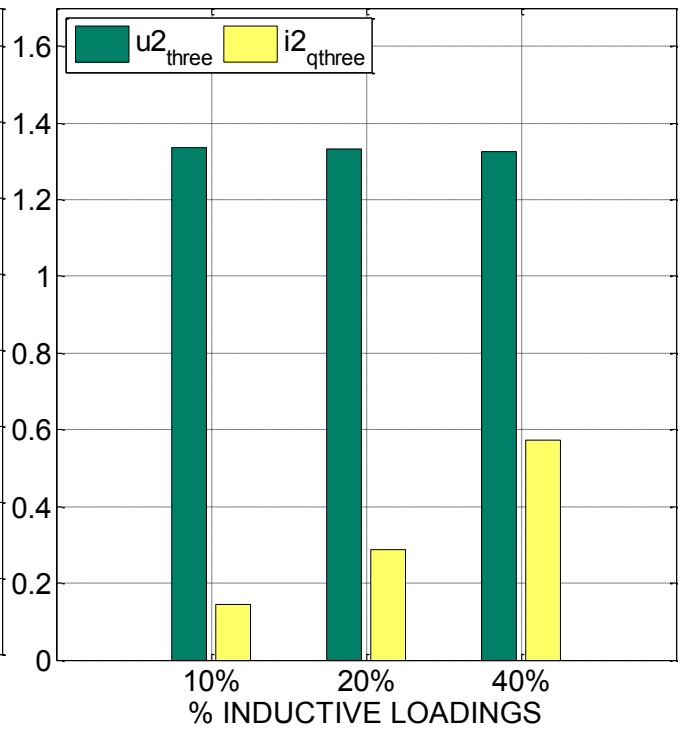


Figure 31: Secondary results for inductive loading.

The y-axis in the above figures represents the secondary voltage (green bar) and the secondary current (yellow bar) in pu. The x-axis corresponds to the different % loading of the transformer. It can be seen in the figures that as the % loading is increasing, the amount of current drawn by the transformer is increasing. Compared to the current, the voltage is rather similar in all of the loading cases.

### 4.1.1.2. Voltage Profile 3

In a similar manner, voltage profile 3 is shown in Figure 32 and its results are plotted in Figure 33 and Figure 34.

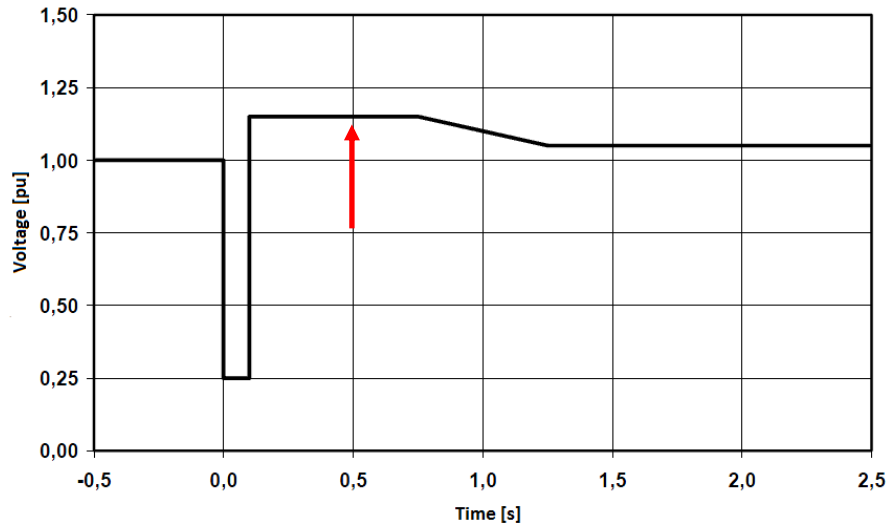


Figure 32: Voltage profile 3 with indication of measurement point.

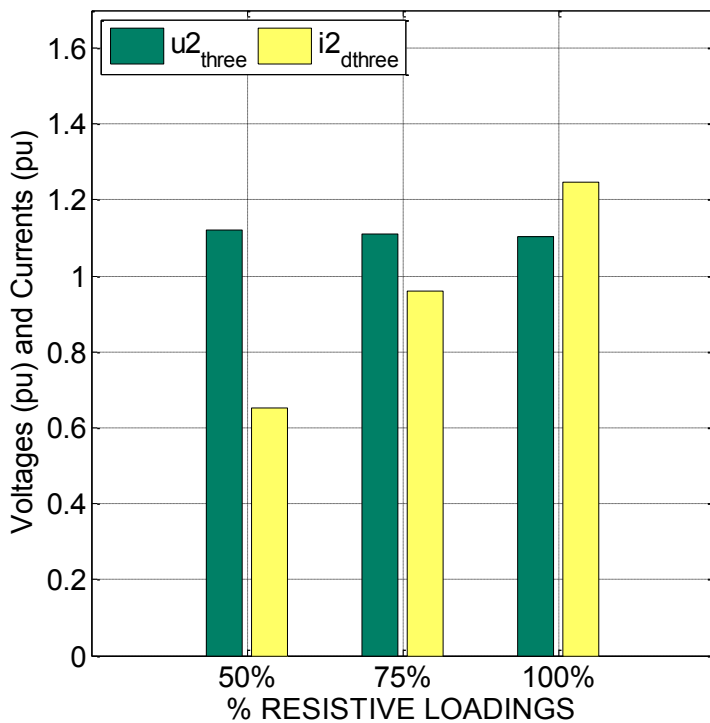


Figure 33: Secondary results for resistive loading.

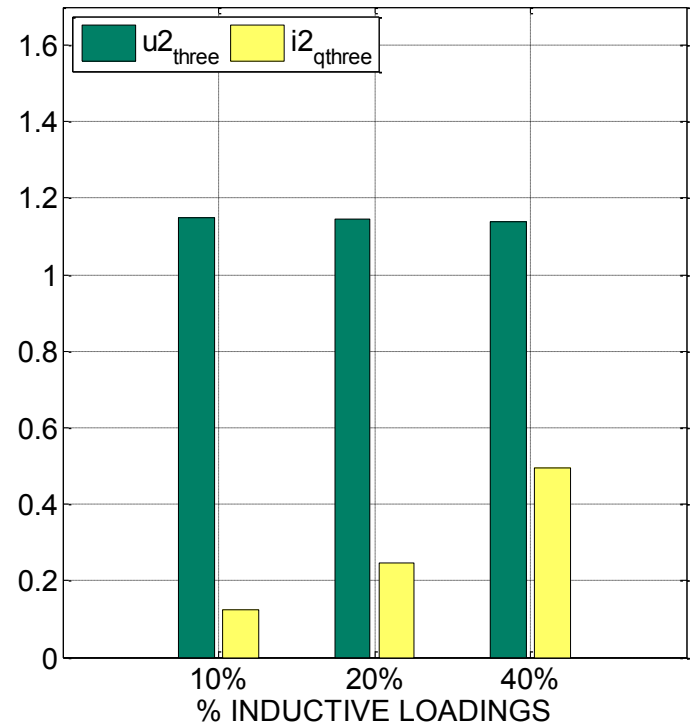


Figure 34: Secondary results for inductive loading.

Here once again the values are taken at the marked point in Figure 32 and one can observe (Figure 33, Figure 34) that with increasing percentage loading, the current is increasing. Similar to the previous case, the secondary voltage is more or less the same.

## 4.2. Comparison between Simulation and Experimentation for 3 Limb Transformer

As was previously mentioned in Chapter 3.5, the model is implemented in MATLAB. All of the cases of experimentation have been performed in the simulations as well to compare and observe the model's effectiveness.

It is interesting to note that all the simulation cases matched quite closely to the experimental results with an overall average error of just 2%. However, there was one exception where the error was a bit more i.e. of voltage profile 2. We will discuss this case and try to clarify why this error occurs.

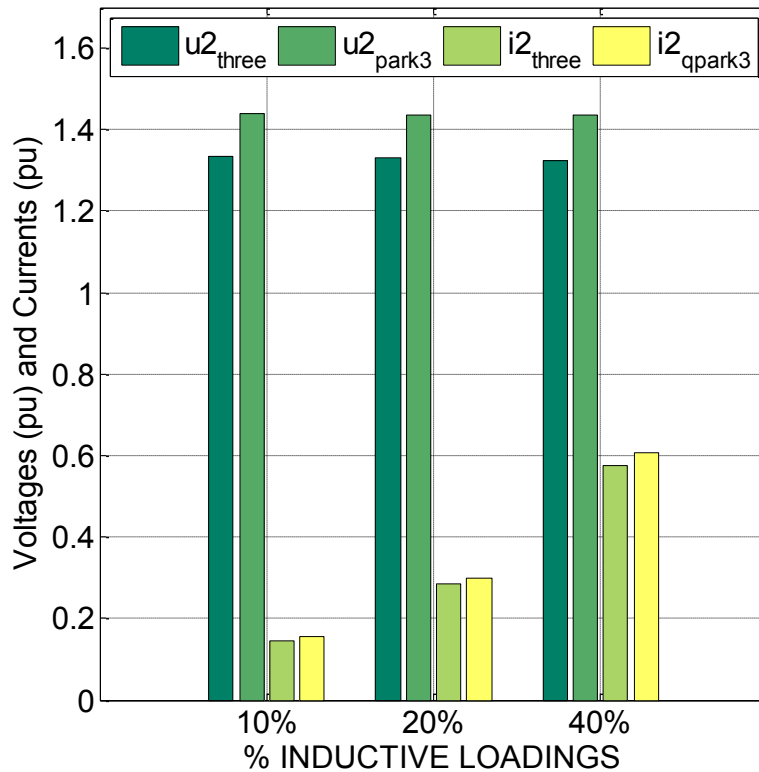


Figure 35: Simulation versus experimental values for voltage profile 2 with inductive loading.

Figure 35 shows % inductive loading on the x-axis and pu values of the secondary voltage and current on the y-axis. The first bar is the secondary voltage for experimentation followed by a simulation. The third bar represents the secondary current in the experiment followed by that of the simulation.

One can observe that the difference in voltage values of simulation compared to experimentation is close to 0.12 pu. The probable cause for this error is the fact that the value of  $L_m$  that is obtained by

experimental values (Figure 14) has its last value corresponding to  $i_m = 6$  A. After this point  $L_m$  remains constant while in actual practice its value does change, the primary current is shown in Figure 41 . Since, the rated current of the primary winding is 5.8 A; therefore it was decided not to go beyond this value.

### 4.3. Comparison between 3 and 5 Limb Experimental results

In this section, we will compare the experimental values of the three limb and five limb transformer.

#### 4.3.1. Voltage Profile 2 – Secondary Voltages

Let’s take the results of voltage profile 2 for comparing a three limb versus a five limb transformer. The results for resistive loading are presented in Figure 36 and for inductive loading in Figure 37 which are taken at the same point as indicated in Figure 29.

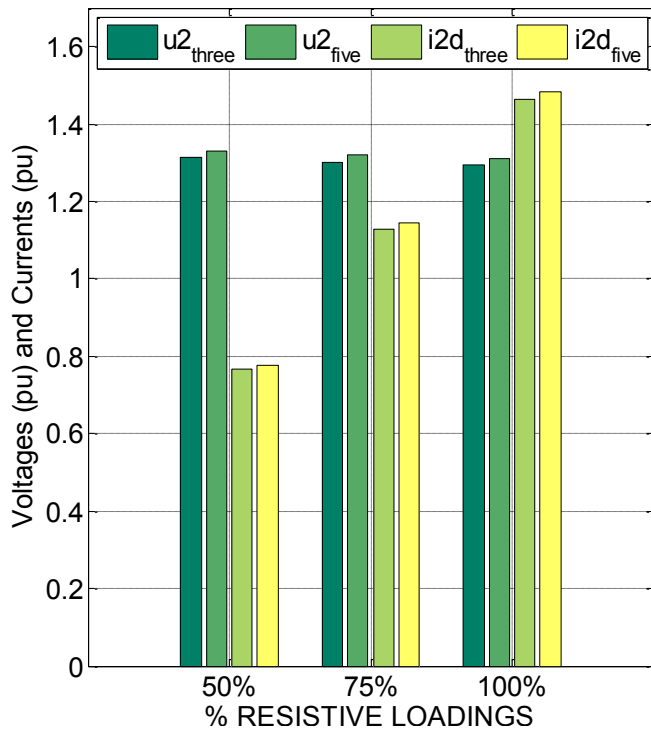


Figure 36: Experimental results for resistive loading.

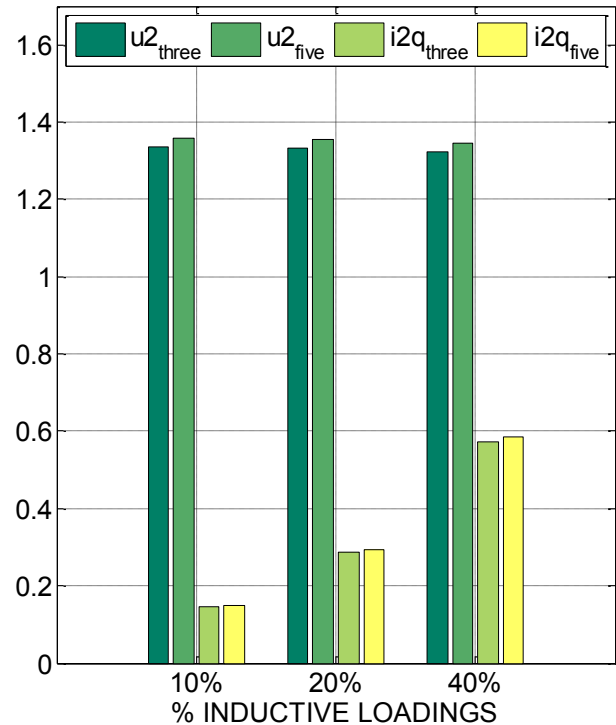


Figure 37: Experimental results for inductive loading.

We can also observe that the current plotted in Figure 36 is only “d” current corresponding to active current for resistive loading while the “q” component (which is not shown here) is zero due to the purely resistive loading. Similarly, in Figure 37 only “q” current is plotted which corresponds to the reactive current drawn by the inductive load.

The results of the secondary voltages for the two types of transformers illustrate that both the voltages and the currents are approximately the same. Interesting results are obtained at the primary side of the transformers which is presented in later sections of the report.

### 4.3.2. Voltage Profile 3 – Secondary Voltages

Considering the results from voltage profile 3 which are plotted at the time instant shown in Figure 32. The values of secondary voltages and currents for different loadings are plotted in Figure 38 and Figure 39

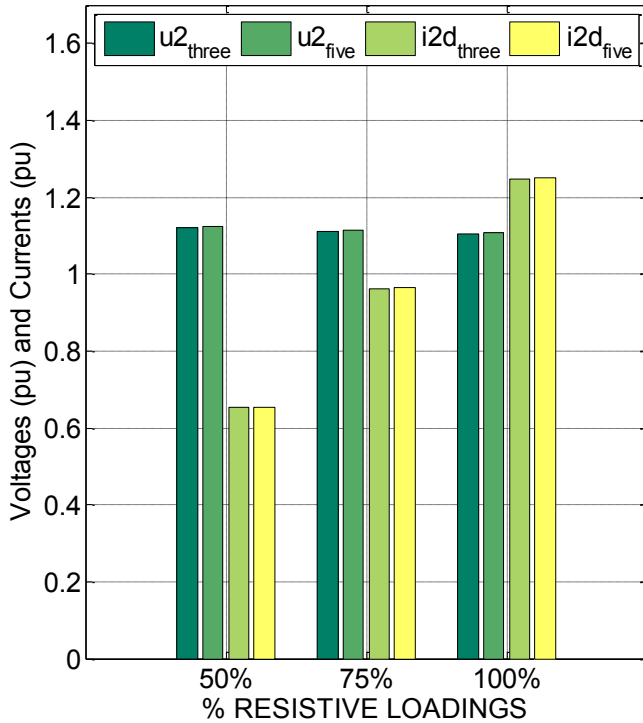


Figure 38: Secondary results for resistive loading.

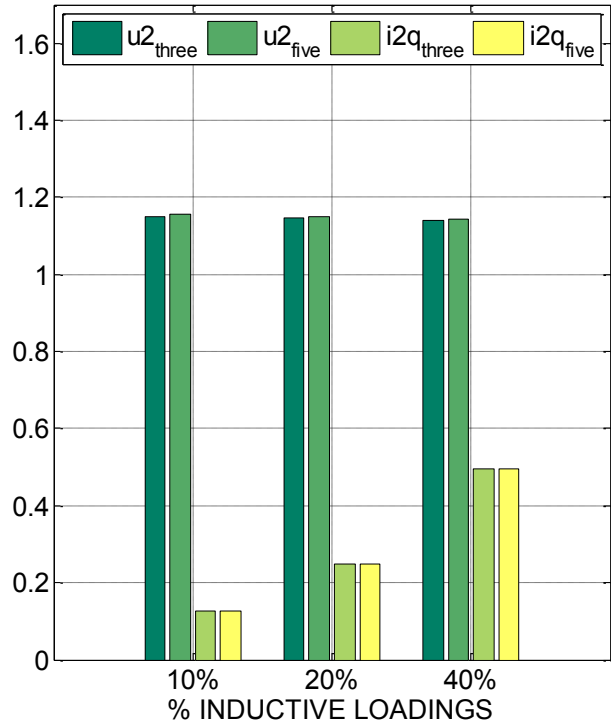


Figure 39: Secondary results for inductive loading.

It is evident from the graphs that the two transformers behave in a similar manner with respect to the voltages and currents. As the percentage loading is increasing; the amount of current drawn by the transformer increases.

### 4.3.3. Voltage Profile 2 – Primary Voltages and Currents

Let us now look at the primary voltages and currents for the two transformer types. There are six sets of bars plotted for each percentage loading. Figure 40 shows the results for resistive loading. It can be observed in the graph that the amount of reactive current drawn by the tree limb transformer is more than for the five limb transformer for all loading cases. Furthermore, it is to be noted that the values are plotted at the time instant marked in Figure 29 which means that both the transformers were saturated at this moment.

For the resistive loading case, it can be observed that when the transformer is lightly loaded (50 % resistive loading), it draws a higher reactive current as compared to the heavily loaded condition (100 %

resistive loading). This also confirms the fact that a lightly loaded transformer is easily saturated as compared to the heavily loaded transformer as is mentioned in [8].

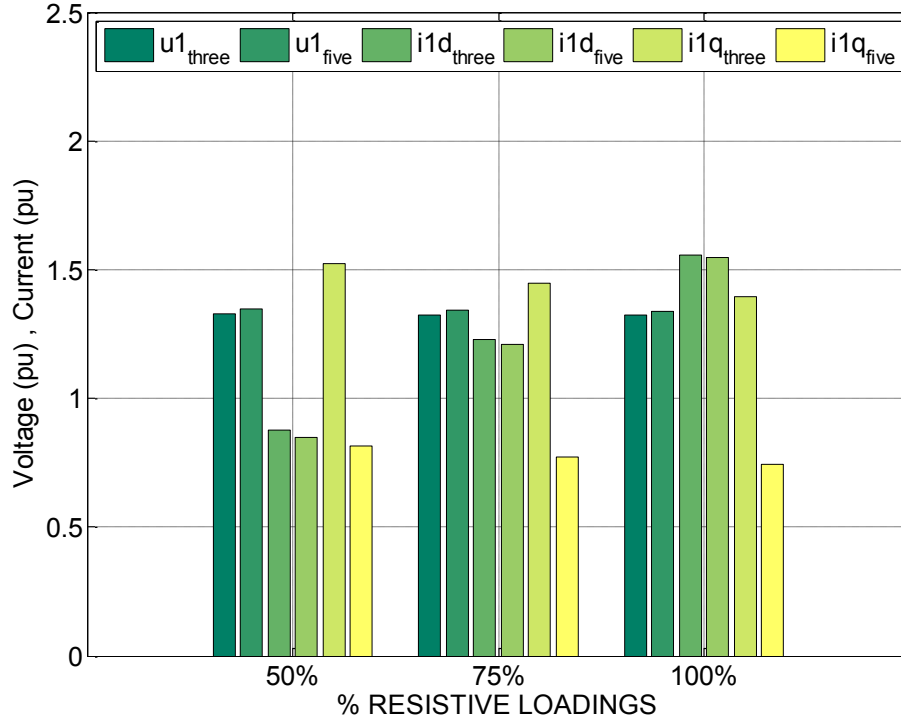


Figure 40: Primary voltages and currents during voltage profile 2 with resistive loading at secondary.

A similar trend is also seen in Figure 41 where the results are plotted for inductive loading. The “q” current for the three limb transformer is greater than for the five limb for all percentage loadings but the trend of reactive current versus % loading is different than for the resistive case. Here, as the % loading is increasing, the reactive current drawn by the transformer is increasing. This can be explained due to the fact that in the equivalent diagram, the inductive load is added to the series branch which is the reason for this increased reactive current.

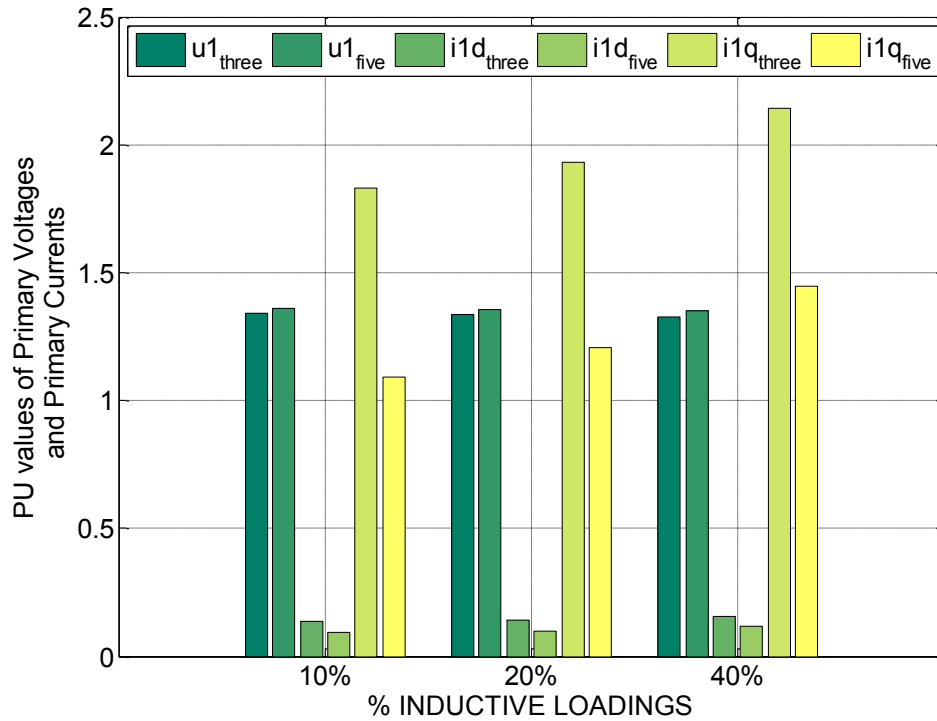


Figure 41: Primary voltages and currents during voltage profile 2 with inductive loadings at secondary.

#### 4.4. Inrush Current Comparison Between 3 and 5 Limb

Previously, we had been looking at the steady state values i.e. when the transients had settled down. It can be interesting to compare the transient behavior of two transformers, when for instance a voltage dip is applied. We will present one case for voltage profile 3 and the values for both three and five limb will be compared at the time instant marked in Figure 42.

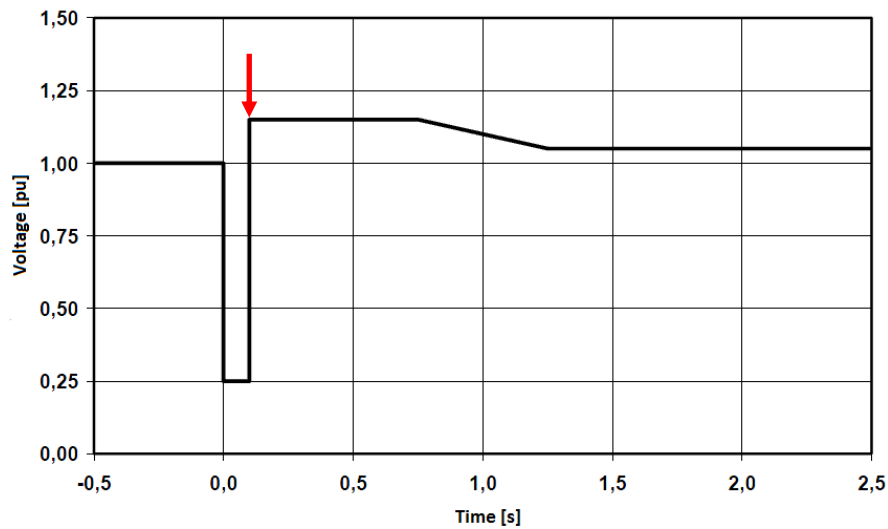


Figure 42: The red arrow indicates the measurement point for the inrush current comparison test.

The results for resistive and inductive loading are plotted in Figure 43 and Figure 44 respectively. In both the figures, one can observe that the three limb transformer draws more current than the five limb transformer for all % loading cases. Comparing the two figures, an important conclusion is that 10 % inductive loading draws a larger current as compared to 50 % resistive loading. The increased amount of current for the inductive loading cases is mainly due to the fact that the inductance of the load tries to recover the voltage at the secondary after the voltage dip has cleared. This in turn saturates the transformer causing the increased current.

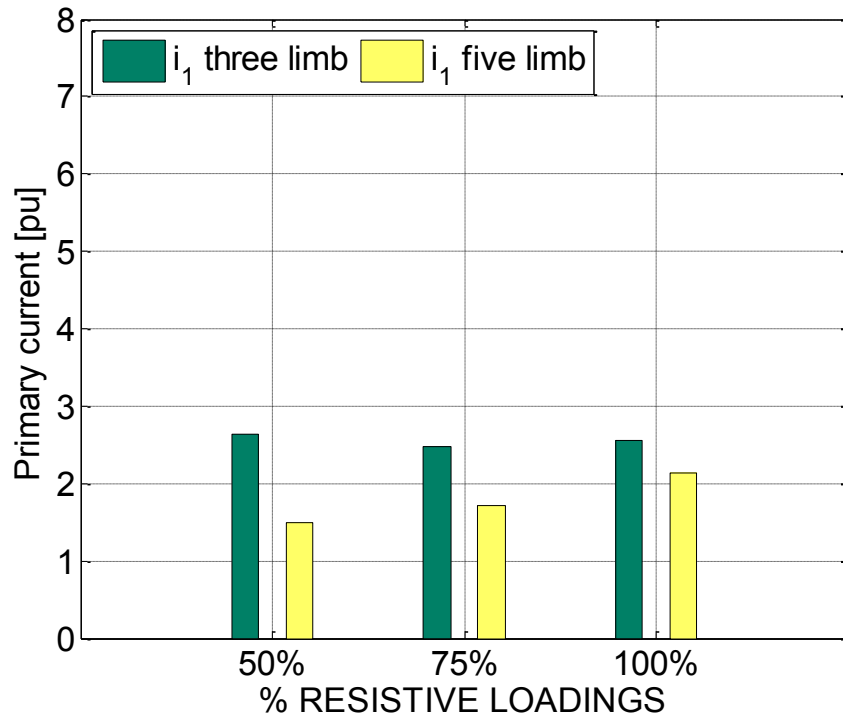


Figure 43: Inrush currents of transformer and its dependence on different resistive loading conditions.

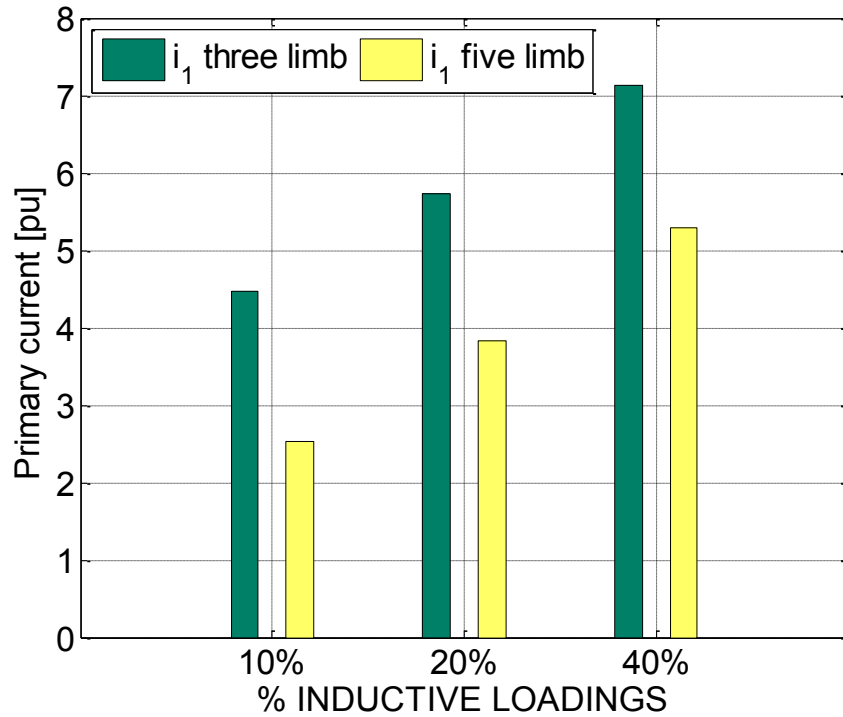


Figure 44: Inrush currents of transformer and its dependence on different inductive loading conditions.

#### 4.5. Window Test

The window test investigates the steady state effect of voltage and frequency variation on the two transformer types. The transformers are operated in open circuit, the voltage was varied between 0.5 pu to 1.5 pu while the frequency was swept from 45 Hz to 55 Hz. For simplicity and ease of comparison, nine points were chosen where results are plotted. Thus at 50 Hz, three readings corresponding to 0.5, 1.0 and 1.5 pu voltage have been analyzed. The same steps are repeated for 45 Hz and 55 Hz. Figure 45 shows the voltage – frequency window with markings of the observation points.

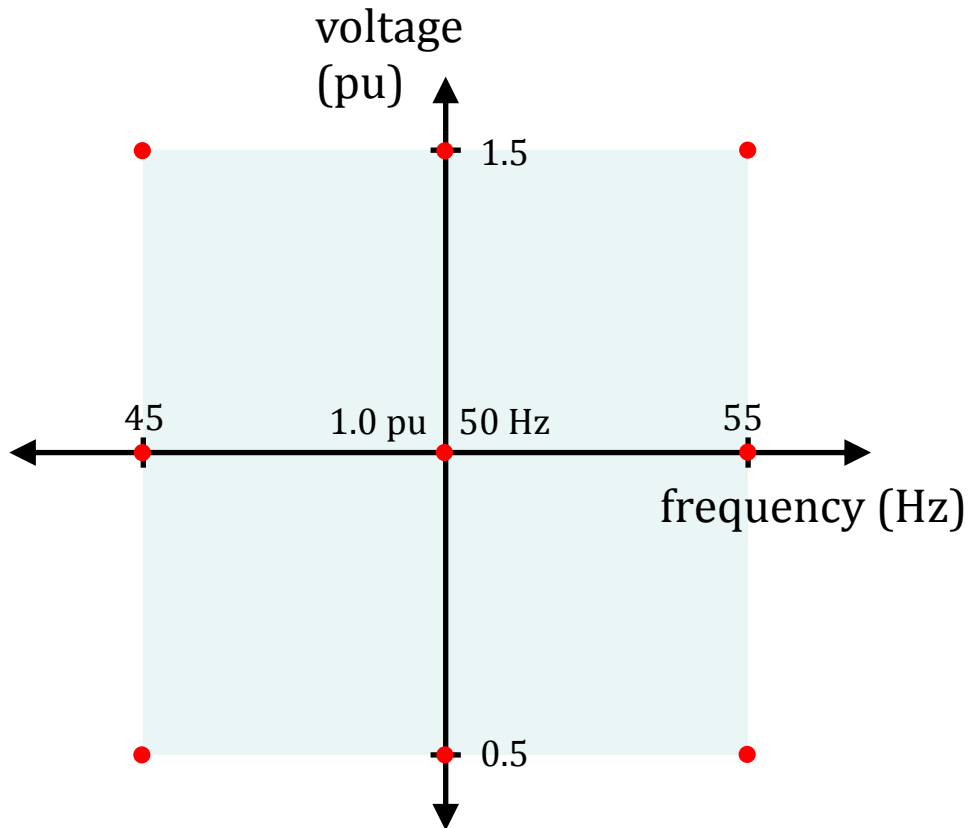


Figure 45: Interesting points for comparison of the transformers behavior.

#### 4.5.1. Comparison of Window Test for 3 Vs 5 Limb

Figure 46 shows the measured results from the window test. It can be seen in the graph that there are nine sets of values. Each set consists of the open circuit currents of the three limbs (blue graphs) and the open circuit current of the five limb (brown graphs) transformer in pu. The first three sets are plotted for 45 Hz followed by 50 Hz and finally 55 Hz. It is clear that 45 Hz with 1.5 pu voltage is the worst case in all the tests. It is because  $V/F$  (voltage / frequency) ratio is the highest in this case. This causes a higher level of flux in the transformer core causing it to go deep into saturation and thus to draw a larger current. If we observe, we can see that three limb transformer draws larger current in open circuit as compared to five limb transformer.

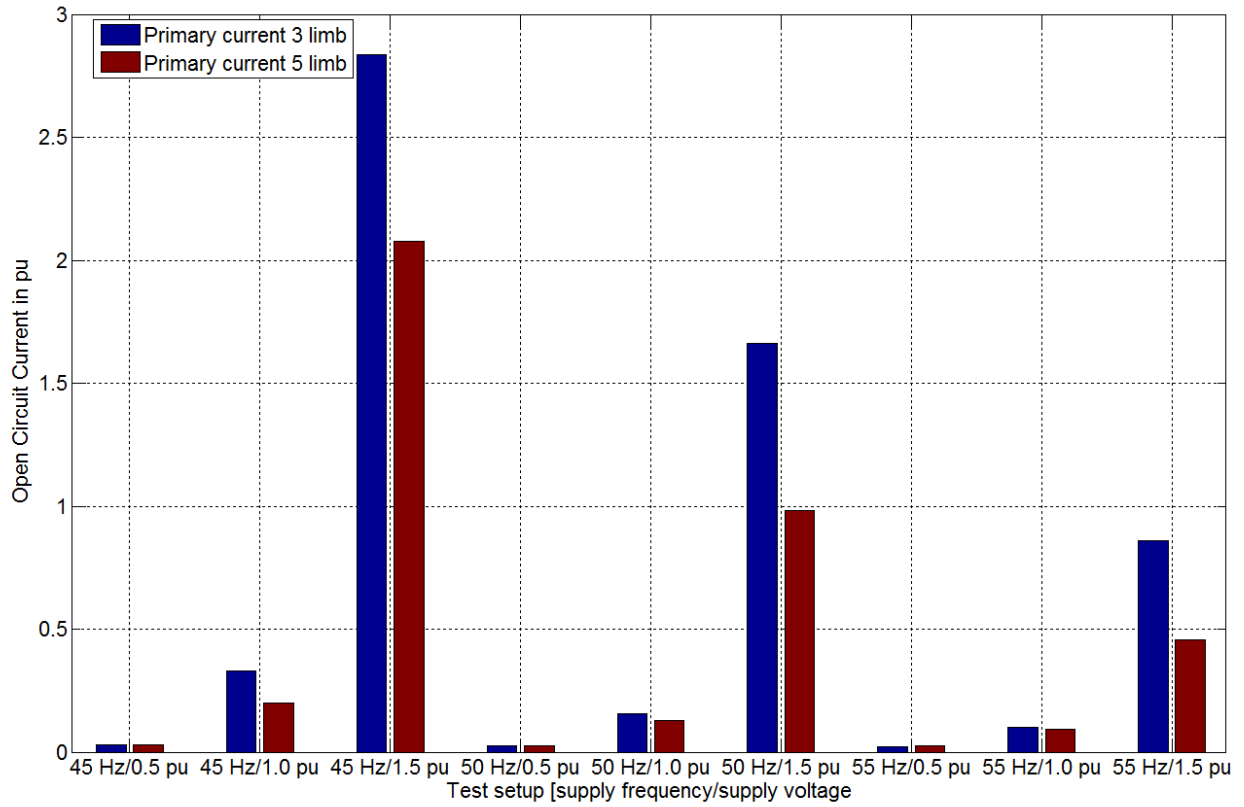


Figure 46: Measured magnetizing current in open circuit and its dependence on supply frequency and voltage.

## 5. Conclusion

From the various voltage profiles it can be deduced that voltage profile number 2 (Figure 5) severely saturates both the transformers. From Chapter 4.3.3 it is apparent that due to the unbalanced flux in the core during this saturated state, the three limb transformer will draw a larger magnetizing current. Compared to this, the outer limbs of the five limb transformer provide a low reluctance path for the unbalanced flux to pass through, which results in a lower magnetizing current.

Voltage profile number 3 (Figure 6) showed very interesting results that were related to the primary current drawn by the two types of transformers. A major difference of inrush current drawn by the two types of transformers was observed when the voltage recovered after the dip. The amount of inrush current and behavior of the transformers was very different depending on the type of loading. For the resistive loading case (Figure 43), the inrush current drawn by the three limb transformer was almost constant for all three loading cases while for the five limb, the current drawn increased gradually. Still, the current drawn by the five limb was lower than that of the three limb transformer. In the case of inductive loadings (Figure 44), one can see that the re-magnetization of the inductive load after the voltage dip, greatly affects the transformer's inrush current. For example, the three limb transformer with 50 % resistive loading case draws a current peak of 2.6 pu while for a similar inductive loading of 40 % it reaches a staggering 7.1 pu. This can be of an issue for the security of the grid [8] which is also mentioned in Chapter 1.2.

Out of all the loading cases, the authors think that the inductive loadings are the worst case and an increase in the resistive part would not cause a further increase of current drawn by the transformers.

If one considers the Voltage-Frequency window in Figure 45, one can observe the correlation between voltage and frequency which is proportional to the flux in the core. This provides a depiction on how the transformers handle the saturation phenomena in a wider range than the cases investigated for different voltage profiles. The tests were performed with the secondary side open; otherwise, the current would be far too large for the rated values of the transformers. It can be observed that throughout the test, the five limb transformer is behaving better than the three limb. This implies that if there is a risk of an overvoltage along with a low frequency, the five limb transformer would be the preferable choice to maintain system security and stability.

The proposed model is working well with an overall average discrepancy between simulated and measured values of 2 %. The limitation of the measurement of  $L_m$  as well as the unbalanced inductive load available for the practical laboratory setup resulted in a larger error than expected for the case of voltage profile 2. However, in other simulation cases, the secondary values which were the focus of this study, behaved very well with low errors. The model however needs the implementation of a hysteresis loop to be more accurate and comparable during the transients of inrush currents.

## 6. Future Work

The curve for  $L_m$  was acquired experimentally for 4 kVA transformers. One interesting topic for future work can be to repeat the same task for a larger transformer e.g. a distribution transformer. One can then apply the current knowledge and fit the new  $L_m$  curve in the existing model. This will help to perform analysis on a larger scale.

In the current Master's thesis, winding connections used for the experiments was wye-wye with floating neutrals at both primary and secondary side. The effect of different winding connections can also be investigated. It will provide a better understanding from the power system point of view.

Voltage profile 3 had a voltage dip duration of 100 ms. The effect of voltage dip duration will be helpful to study the response and behavior of these different types of transformers.

This Master's thesis which was performed on transformers was a second part of an investigative study initiated by OKG AB. The first part which was based on the response of asynchronous machines was undertaken and completed by Johan Andersson [23]. So, finally it would be very interesting to combine both these parts together and perform an overall system study of the network including both the transformers and induction machines.

## References

- [1]: Bruce A. Mork, Francisco Gonzalez, Dmitry Ishchenko, Don L. Stuehm and Joydeep Mitra, "Hybrid Transformer Model for Transient Simulation—Part I: Development and Parameters", *IEEE TRANSACTIONS ON POWER DELIVERY*, VOL. 22, NO. 1, JANUARY 2007.
- [2]: Bruce A. Mork, Francisco Gonzalez, Dmitry Ishchenko, Don L. Stuehm and Joydeep Mitra, "Hybrid Transformer Model for Transient Simulation—Part II: Laboratory Measurements and Benchmarking", *IEEE TRANSACTIONS ON POWER DELIVERY*, VOL. 22, NO. 1, JANUARY 2007.
- [3]: David Ribbenfjärd, "Electromagnetic transformer modeling including the ferromagnetic core", *KTH, ISBN 978-91-7415-674-4, SWEDEN 2010*.
- [4]: M. R. Dolatian and A. Jalilian, "Voltage Sag Effect on Three Phase Five Leg Transformers", *World Academy of Science, Engineering and Technology 28, Department of Electrical Engineering, Iran University of Science & Technology, Tehran, Iran 2007*.
- [5]: Joaquín Pedra, Luis Sáinz, Felipe Córcoles and Luis Guasch, "Symmetrical and Unsymmetrical Voltage Sag Effects on Three-Phase Transformers", *IEEE TRANSACTIONS ON POWER DELIVERY*, VOL. 20 NO. 2, APRIL 2005.
- [6]: Jialong Wang and Raluca Lascu, "Zero Sequence Circuit of Three-legged Core Type Transformers", Basler Electric Company, USA.
- [7]: R.S. Bhide, S.V. Kulkarni, P.B. Bhandarkar, "Analytical description for zero-sequence characteristics of five-legged core construction in transformers", *IET Electric Power Applications*, ISSN 1751-8660, India 2009.
- [8]: Emmanouil Styvaktakis, Math Bollen, Irene Y.H., "Transformer saturation after a voltage dip", *IEEE Power Engineering Review*, 20 ( 4 ) s. 62-64 2000.
- [9]: Transformer Engineering Design and Practice by Khaparde & Kulkarni pp 36-38.
- [10]: Current and power relationship in the measurement of iron losses in a three phase three limb transformer core by Brailsford (1954)
- [11]: J&P Transformer Book 12th edition, 1998, ISBN 07506 1158 8, p 107
- [12]: Zero Sequence Circuit of Three-legged Core Type Transformers Jialong Wang (Basler Electric), Raluca Lascu (DTE Energy)
- [13]: Transformer Engineering Design and Practice by Khaparde & Kulkarni , pp 109-111

- [14]: J&P Transformer Book 12th edition, 1998, ISBN 07506 1158 8, p 32
- [15]: J&P Transformer Book 12th edition, 1998, ISBN 07506 1158 8, p 41-42
- [16]: Electromagnetic Transformer modeling including the ferromagnetic core, David Ribbenfjärd, Sweden 2010, KTH. pp 16-18
- [17]: ABB Transformer Handbook p 142
- [18]: Rapport Oskarshamn 3 – Underlag till referensrapport SAR Allmän del – Störningstålighet hos komponenter i hjälpkraftsystemet vid störningar från yttre nät
- [19]: David W. Johnson (2000). "EGR 325, Electromechanics Technical Paper #2". Grand Valley State University.
- [20]: Torbjörn Thiringer (1996). "Measurements and Modelling of Low-Frequency Disturbances in Induction Machines". Chalmers University of Technology.
- [21]: Carlson, Ola (1988). "Analys av synkrogenerator med frekvensomriktare för elgenerering vid variabelt varvtal".
- [22]: MathWorks, "State-Space Models",  
<http://www.mathworks.se/help/toolbox/control/ug/bsuyp98.html#bsuyu0h>, fetched 2011-09-08.
- [23]: Modeling and Measurements of the Response of Asynchronous Machines Exposed to Voltage Dips  
By Johan Andersson
- [24]: LeCroy, "WaveSurfer® MXs-B and MSO MXs-B Oscilloscopes", Manual, *WSMXs-B-MSO-MXs-B-DS-19Jan11*.
- [25]: LeCroy, "AP031/AP032 Differential Probe Operating Instructions", AP031/032-OM-E Revision B - November 1996.
- [26]: LeCroy, "Current Probes - Accurately AP015 – 30 A, 50 MHz Current Probe", DCCP - 07/05.

## Appendix A. Parameter Extraction

### Rating plate

The rating plates are as follows:

#### 67128 – 5 limb transformer

Isolating transformer by Noratel Sweden AB

Art. no. 5-080-000688

Acc. to. EN61558-2-4 ,  $t_a=25$  degrees C

TYPE 3LT-00-4,0

4000VA

Input/pri.: 230 V<sub>L-N</sub> 6,2A III

Output/sec.: 115 V<sub>L-N</sub> 5,8A III , 115 V<sub>L-N</sub> 5,8A III

Insul. cl.: F     Duty: Cont.     Cooling: AN     Built: 2011

#### 67129 – 3 limb transformer

Isolating transformer by Noratel Sweden AB

Art. no. 5-080-000687

Acc. to. EN61558-2-4 ,  $t_a=25$  degrees C

TYPE 3LT-00-4,0

4000VA

Input/pri.: 230 V<sub>L-N</sub> 6,2A III

Output/sec.: 115 V<sub>L-N</sub> 5,8A III , 115 V<sub>L-N</sub> 5,8A III

Insul. cl.: F     Duty: Cont.     Cooling: AN     Built: 2011

### Open circuit test

The test was performed with the following connection Figure 47 on transformer unit #67128 and #67129.

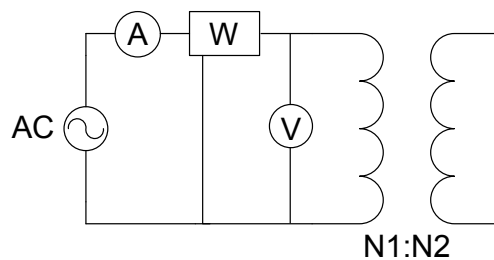


Figure 47: Open circuit test.

**Table 5: Results from open circuit test.**

Transformer	V <sub>oc</sub> (L-N) [V]	I <sub>oc</sub> [A]	P <sub>sc-3</sub> (3-phase) [W]
67128 – 5 limb	231	0.43	48
67129 – 3 limb	230	0.41	71

The primary winding was Y-connected and the neutral point grounded. Secondary was an open circuit.

### Short circuit test

The test was performed with the following connection Figure 48 on transformer unit #67128 and #67129.

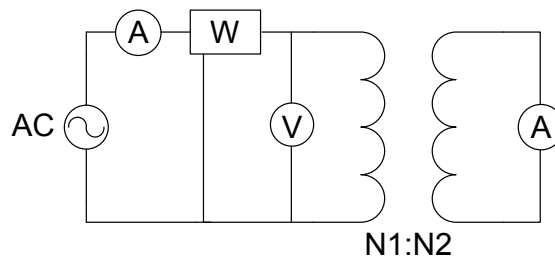


**Figure 48: Short circuit test.**

**Table 6: Results from short circuit test**

Transformer	V <sub>sc</sub> (L-N) [V]	I <sub>sc</sub> [A]	P <sub>sc-3</sub> (3-phase) [W]
67128 – 5 limb	4	6.14	70
67129 – 3 limb	4.4	5.78	69

The primary winding was Y-connected and the neutral point grounded. Secondary winding was short circuited.

### Calculations

$$R_M = \frac{V_{oc}^2}{P_{oc}} \quad (\text{equ. 1})$$

$$X_M = \sqrt{\left(\frac{I_{oc}}{V_{oc}}\right)^2 - \frac{1}{R_M^2}} \quad (\text{equ. 2})$$

$$R_{eq} = \frac{P_{sc}}{I_{sc}^2} \quad (\text{equ. 3})$$

$$X_{eq} = \sqrt{\left(\frac{V_{sc}}{I_{sc}}\right)^2 - R_{eq}^2} \quad (\text{equ. 4})$$

This results in the following table:

**Table 7: The parameters determined from the transformers**

<b>Parameter</b>	<b>5-limb [<math>\Omega</math>]</b>	<b>3-limb [<math>\Omega</math>]</b>
$R_{eq}$	0.61	0.69
$R_M$	3351	2235
$X_{eq}$	0.20	0.32
$X_M$	544.31	579.52

### **Magnetizing inductance test**

An open circuit test (see Figure 47) was then performed where the voltage was increased from 70 V to the appropriate voltage. Voltage was increased in steps of 5-10 V, depending on the need for accuracy, until rated current was reached.

To make sure that the zero sequence current could propagate, since the open circuit test is highly unbalanced condition, the generators neutral point was solidly grounded as well as the neutral point for the primary on the transformer. This removed the issue with floating Y-point potential, although the earth protection sensor had to be disconnected in the switch gear.

The results were as follows:

Table 8: Results from 3-limb transformer at 50 Hz in an open circuit test.

Test	V <sub>r</sub> [V]	P [W]	I [A]
1	11	0,549	0,063
2	17,5	1,1	0,073
3	23,85	1,6	0,082
4	26,6	2	0,086
5	33	2,8	0,093
6	36,6	3,2	0,103
7	40,2	3,8	0,109
8	42,8	4,2	0,114
9	48,8	5,2	0,126
10	52	6	0,13
11	58,17	7,81	0,16
12	60	8,65	0,168
13	63,8	9,09	0,18
14	67,7	10,01	0,188
15	70,5	11,15	0,202
16	72,8	12,24	0,221
17	76	13,58	0,239
18	78	15,02	0,258
19	81,17	16,58	0,281
20	84,32	18,6	0,303
21	86,6	20,48	0,327
22	90	22,9	0,363
23	92,5	25,4	0,393
24	95,35	28,35	0,435
25	101	35,1	0,52
26	106,8	44,8	0,64
27	111	56,9	0,79
28	118,6	79,1	1,02
29	124,8	111	1,407
30	130,6	170	2,06
31	136	259	2,97
32	142	387	4,31
33	147,7	558	6

Table 9: Results from 5-limb transformer at 50 Hz in an open circuit test.

Test	Vr [V]	P [W]	I [A]
1	7,36	0,228	0,04372
2	10,78	0,407	0,0488
3	15	0,714	0,0588
4	17,6	0,947	0,0647
5	22,41	1,4	0,0701
6	24,16	1,67	0,0782
7	27	1,94	0,0812
8	31	2,4	0,0884
9	33	2,92	0,0971
10	38	3,49	0,103
11	40,7	4	0,109
12	43,9	4,67	0,1164
13	47,2	5,31	0,1233
14	53	6,5	0,135
15	55,6	7,48	0,145
16	60,27	8,4	0,1498
17	62,9	9,04	0,1621
18	66,2	10,16	0,1701
19	68,9	11,02	0,184
20	74,7	13,12	0,209
21	78,7	14,8	0,231
22	80,7	15,8	0,2417
23	83,7	17,58	0,2628
24	86,9	19,3	0,2854
25	89,67	20,9	0,3114
26	96	25,6	0,3621
27	101,7	30,6	0,4294
28	108	37,27	0,5121
29	114,48	44,9	0,62
30	121,2	53	0,73
31	128	62,5	0,855
32	143	94,1	1,32
33	151	115,9	1,67
34	160	148	2,25
35	168,5	193	3,16
36	177,5	252	4,49
37	186	340	6,2

## Appendix B. Measurement Devices

This part of the appendix describe the different measurement devices that were used during the open circuit test, the short circuit test as well as the configuration of the measurement boxes used during the practical experimentation.

The oscilloscope used during the calibrations and tests was the LeCroy 24MXs-B seen in Figure 49.



Figure 49: Picture of the LeCroy 24MXs-B Oscilloscope used to get the readings from the probes and to calculate the input power.

Table 10: Parameters for LeCroy 24MXs-B Oscilloscope

Bandwidth (@50 ohm)	200 MHz
Rise Time	1.75 ns
Input channels	4
BW Limit	20 MHz
Sample Rate (Single shot)	2.5 GS/s
Sample Rate (Repetitive)	50 GS/s
Display Type	Color, 10.4" TFT-LCD Touch Screen

[24].

The voltage differential probe used for the experiments was the LeCroy AP032 seen in Figure 50.

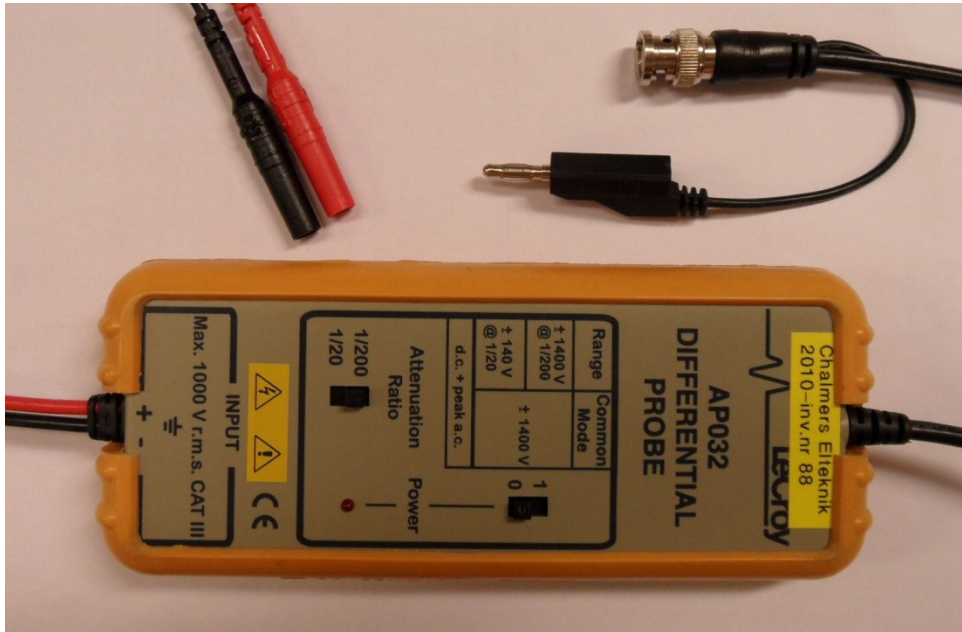


Figure 50: Picture of LeCroy AP032 voltage differential probe and its connections.

Table 11: Parameters for LeCroy AP032 voltage differential probe [25].

Bandwidth	25 MHz
Rise Time	14 ns
Attenuation	1:20/1:200
Accuracy	$\pm 2\%$
Power req.	4 1.5 V AA size batteries or 6 V <sub>dc</sub> adapter

The current probe used for the experiments was the LeCroy AP015 seen in Figure 51.

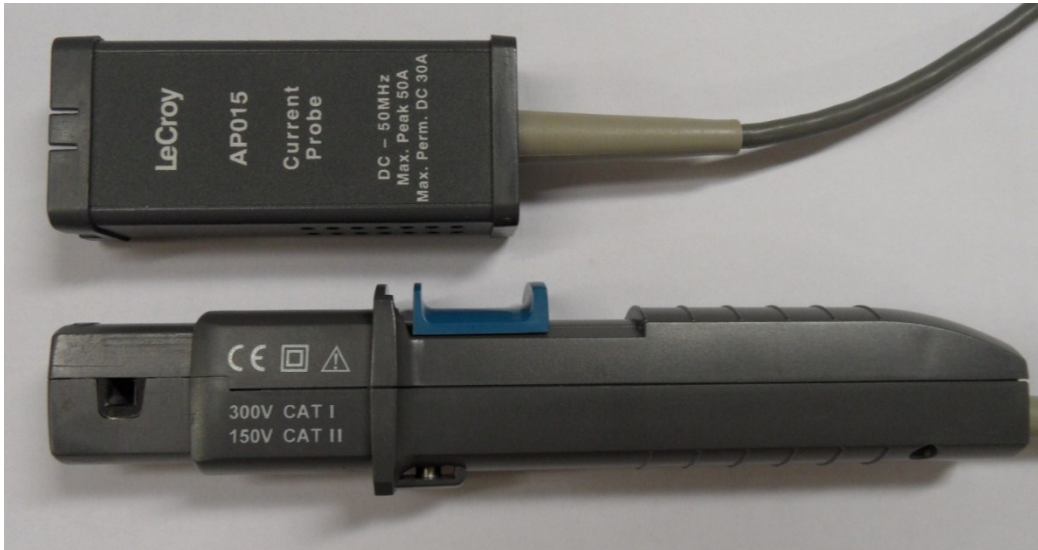


Figure 51: LeCroy AP015 current probe.

Table 12: Parameters for LeCroy AP015 current probe [26].

Bandwidth	50 MHz
Max. Cont. Current	30 A
Max. Peak Current	50 A < 10 s
Accuracy	±1 %
Min. Sensitivity	10 mA/div

# Appendix C. Additional Results

Here are the additional secondary experimental results presented for the voltage profile 1 and 4 as well as the primary plots of voltage profile 1, 3 and 4.

First let's revise the profiles and the chosen point for these results:

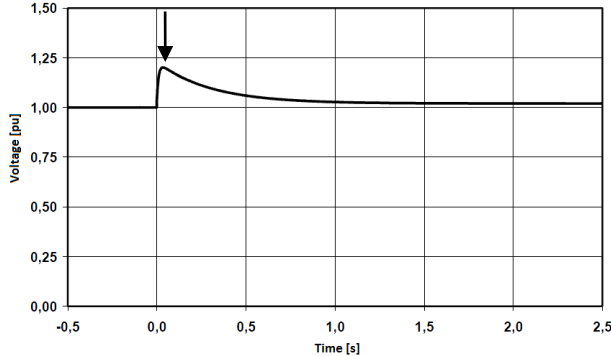


Figure 52: Voltage profile 1

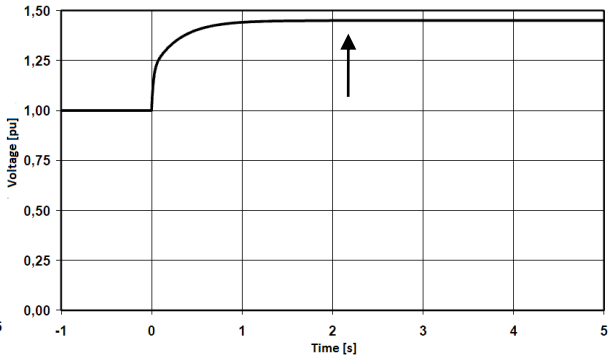


Figure 53: Voltage profile 2

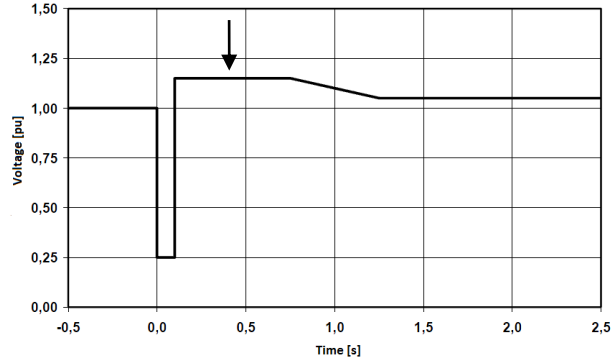


Figure 55: Voltage profile 3

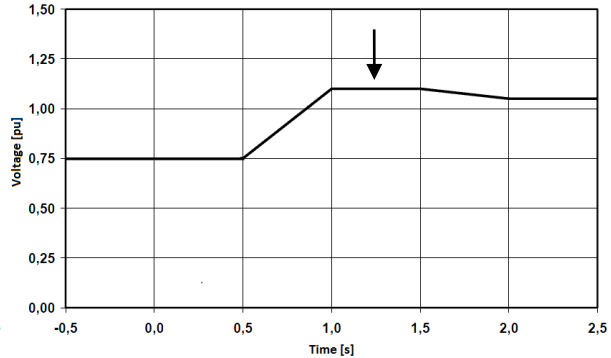
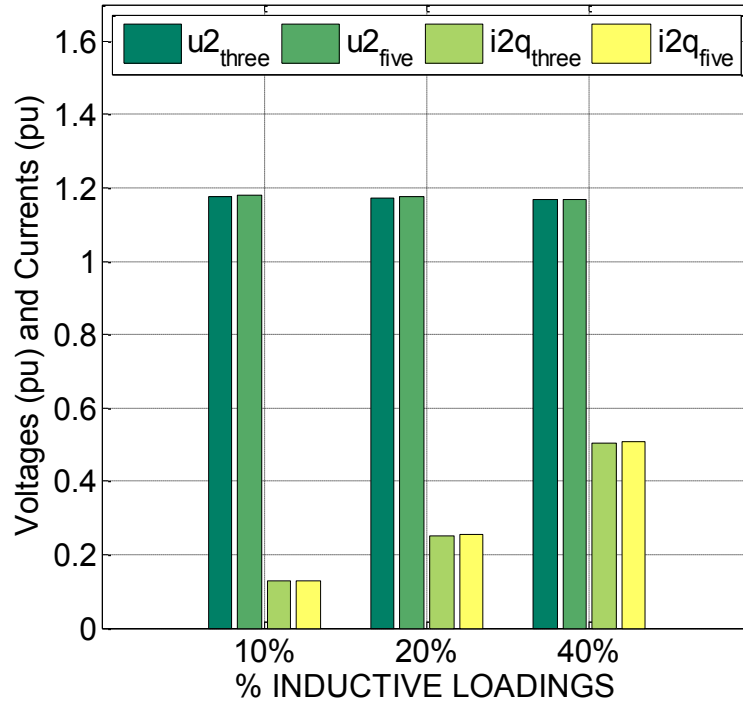


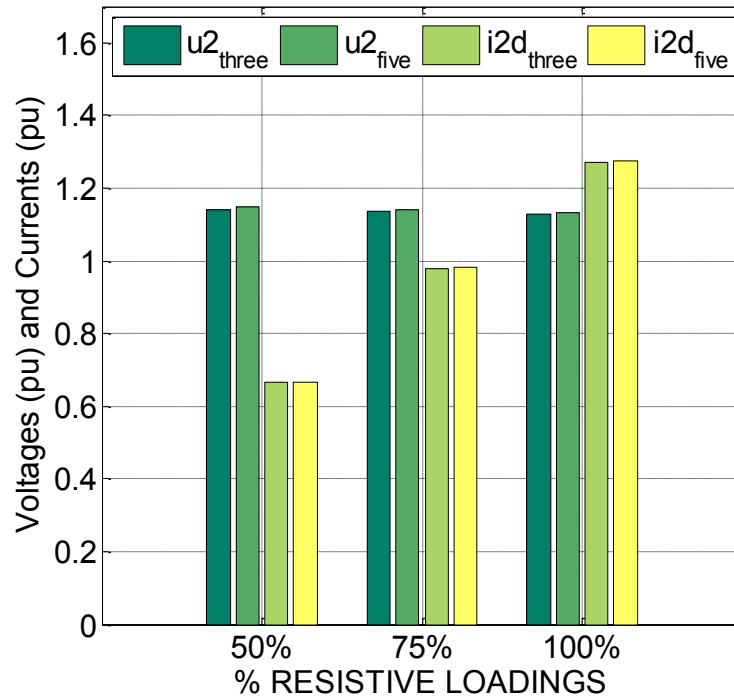
Figure 54: Voltage profile 4

## Voltage profile 1 - Secondary results comparison between three and five limbed transformer.

### Inductive loading

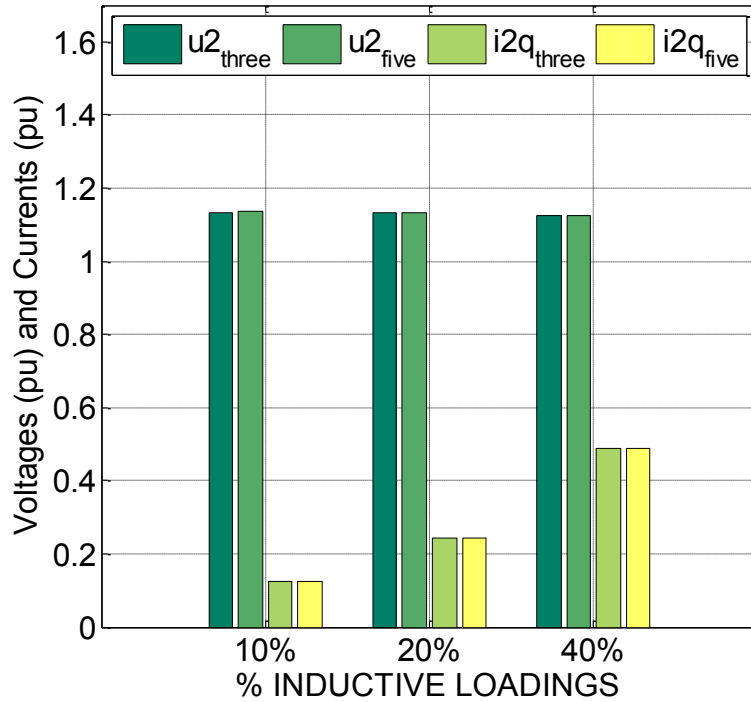


### Resistive loading

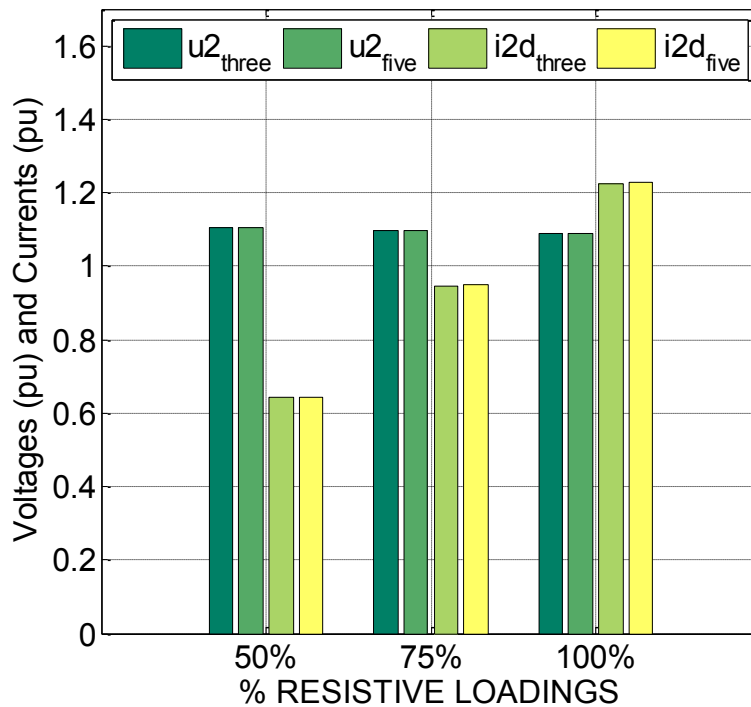


## Voltage profile 4 – Secondary results comparison between three and five limbed transformer.

### Inductive loading

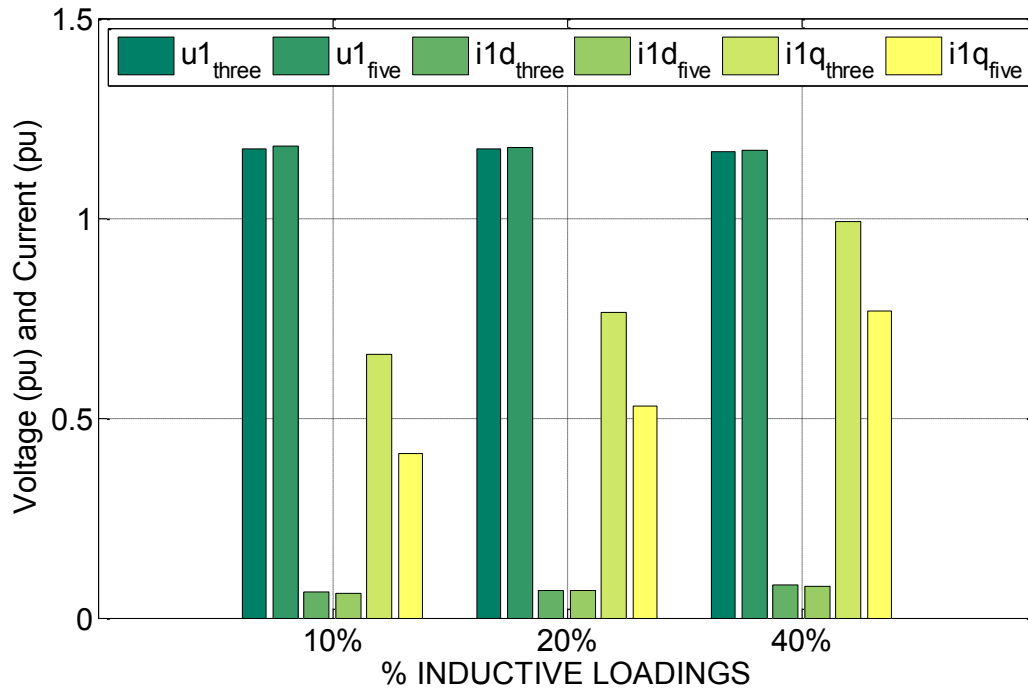


### Resistive loading

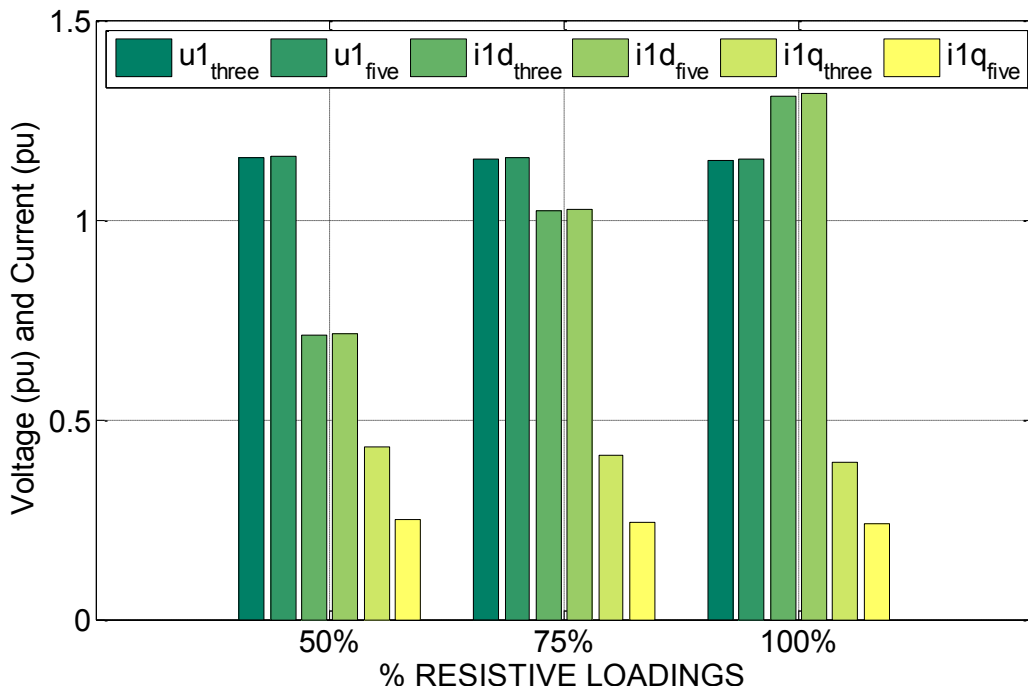


## Voltage profile 1 - Primary results comparison between three and five limbed transformer.

### Inductive loading

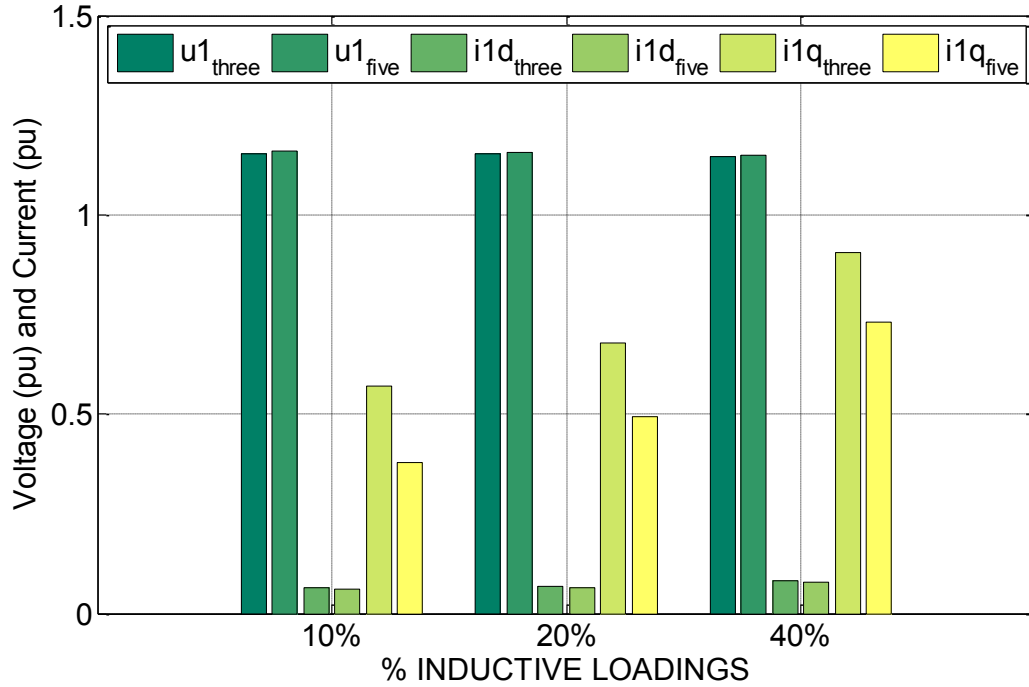


### Resistive loading

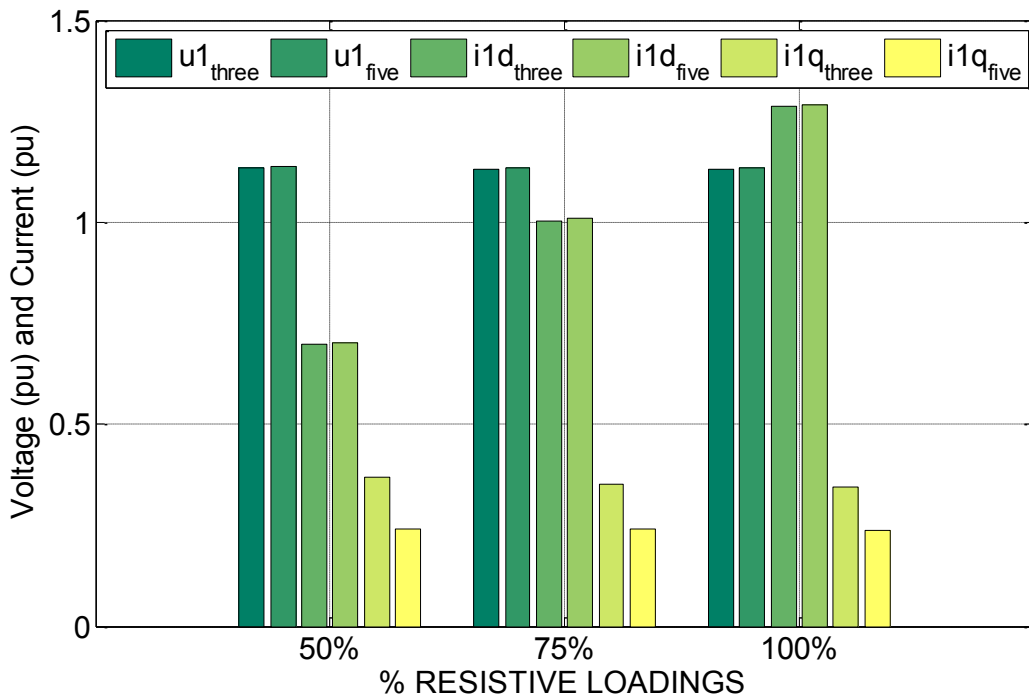


## Voltage profile 3 - Primary results comparison between three and five limbed transformer.

### Inductive loading

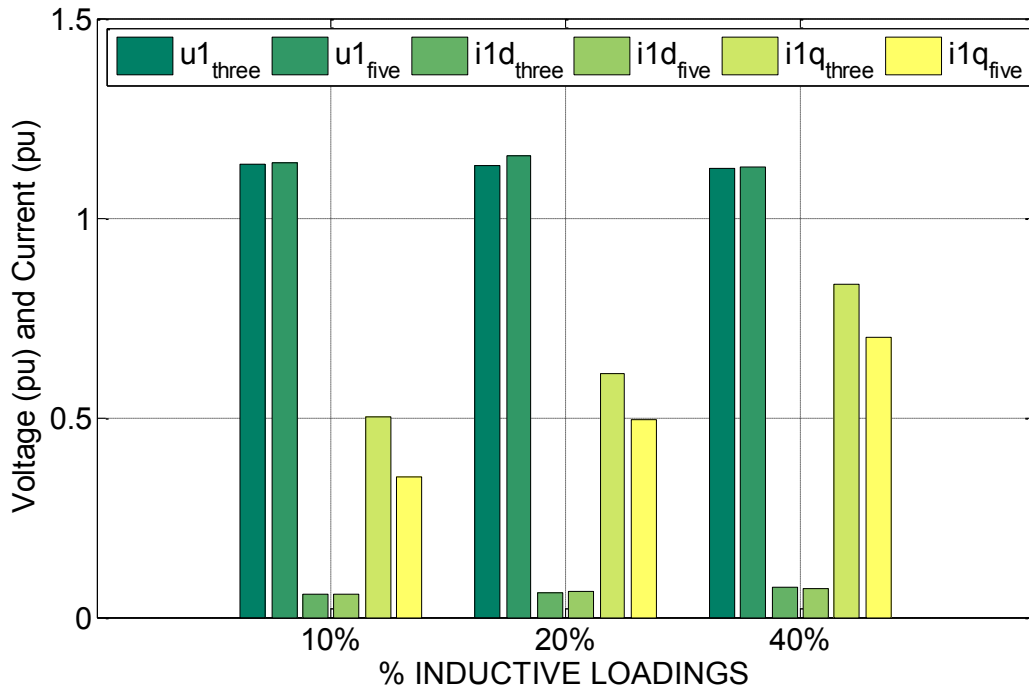


### Resistive loading



## Voltage profile 4 - Primary results comparison between three and five limbed transformer.

### Inductive loading



### Resistive loading

